GRAY GROUP

Two Stage to Orbit Design

June 1991

Gray Group

By:

Carrier Team:

Dan Ensminger- Team Leader, Carrier Section Editor
David Groat- Weights & Balances, Model
Matt Manifold- Aerodynamics
Kevin Patton- Propulsion
Steve Pellican- Trajectory, Propulsion
Eric Bish*- Heat Transfer
Steve Boham*- Waverider Aerodynamics
Tor Dietrichs*- Trajectory, Supersonic Aerodynamics
Jeff Poling*- Stability & Control

Orbiter Team:

Peter Lee- Team Leader, Orbiter Section Editor
Dan Aug- Heat Transfer
Bob Cleaves- Aerodynamics, Stability & Control
Jim Giuliani- Trajectory
Ed Marin- Propulsion
Matt Urbancic- Stability & Control
J.B. Cunningham*- Trajectory
Dan Pheils*- Stability & Control
Matt Streby*- Trajectory, Ergonomics

*- Team member Winter Quarter only

OSU/USRA Senior Design

Submitted for:
The Ohio State University
Department of Aeronautical and
Astronautical engineering
Spring 1991

ABSTRACT

A preliminary design of a two-stage to orbit vehicle was conducted with the requirements to carry a 10,000 pound payload into a 300 mile low-earth orbit using an airbreathing first stage, and to take off and land unassisted on a 15,000 ft runway.

The goal of the design analysis was to produce the most efficient vehicle in size and weight which could accomplish the mission requirements. Initial parametric analyses indicated that the weight of the orbiter and the transonic performance of the system were the two parameters that had the largest impact on the design.

The resulting system uses a turbofan-ramjet powered first stage to propel a scramjet and rocket powered orbiter to the stage point of Mach 6 to 6.5 at an altitude of 90,000 ft.

Table of Contents

LIST OF FIGURES

LIST OF TABLES

1. Introduction.

The proposed existence of a permanent manned space station would necessitate an efficient means of transportation to and from the station. The Space Shuttle remains an excellent and versatile system for taking large payloads into orbit, but a smaller, more efficient system would need to be devised for taking small, routine payloads such as men and supplies into space.

The two-stage to orbit concept is a very viable idea for fulfilling these requirements. It is much smaller and more efficient for small payloads than the Space Shuttle, and it is possibly more attainable and near term than a single-stage to orbit vehicle such as the NASP. Even a system with a scramjet powered second stage would be easier to accomplish than the NASP, since the vehicle will be accelerated to a Mach number at which the scramjets can operate, and the effective heating time on the ascent would be reduced since the orbiter is protected by the carrier on the ascent phase.

Placing a 10,000 lb payload in a 300 mile low earth orbit was assigned as the primary requirement in order to accomplish the mission of space station shuttle as described. The first stage was constrained to make use of airbreathing propulsion, and to be able to takeoff and land on 15,000 ft. runways.

2. Summary.

The primary design goal was to meet the mission requirements with a design which is safe and efficient. In addition, we set other design requirements for ourselves: that the carrier be able to return to the launch site with the orbiter in the case of an aborted separation, and that the carrier have some capacity to ferry the orbiter between launch and/or recovery sites.

A "general-to-specific" design philosophy was adopted in order to make the best use of our time. Detailed analyses were only carried out after initial parametric studies were conducted in order to determine the portions of the design deserving the most of our attention. The gross takeoff weight was found to be a strong function of transonic performance and of the orbiter weight, and these parameters shaped the rest of our design.

The staging point was one of the most important considerations of the design. The staging point between Mach 6 and Mach 6.5 at 90,000 ft was chosen for a number of reasons. The Mach number chosen was a balance between minimum orbiter weight and carrier complexity. Staging at higher Mach numbers required more heat protection and more elaborate propulsion systems for the carrier, removing the benefit of the reduced orbiter weight. The staging altitude was a balance between orbiter scramjet engine performance and carrier maximum dynamic pressure limits for staging. A higher altitude would significantly reduce the thrust and lift of the orbiter at staging, possibly causing the orbiter to fall back onto the carrier after separation.

The trajectory drove much of the design for this project. The Gray Group has designed the trajectory to use minimum fuel over the entire flight and to reduce aerodynamic heating after stage. In order to use less fuel, the carrier must compromise between flying at a high altitude for low drag and flying at a low altitude for high thrust. The last two quarter's work has culminated in our present time-stepping trajectory analysis programs which utilize General Electric study engine data and modified experimental aerodynamic data.

The initial shape analyzed for the carrier was a waverider, as shown in Figure 2.1. The waverider was chosen initially because of the high L/D's possible near the stage point. However, our Winter quarter analysis showed that the high L/D's were not attained throughout our flight regime, and that the increase in performance at high Mach numbers had negligible affect on the take-off weight compared to the transonic performance. In addition, the waverider configuration was difficult to trim at takeoff and landing, and several modifications would have been required.

This quarter we began a new design based on what we had

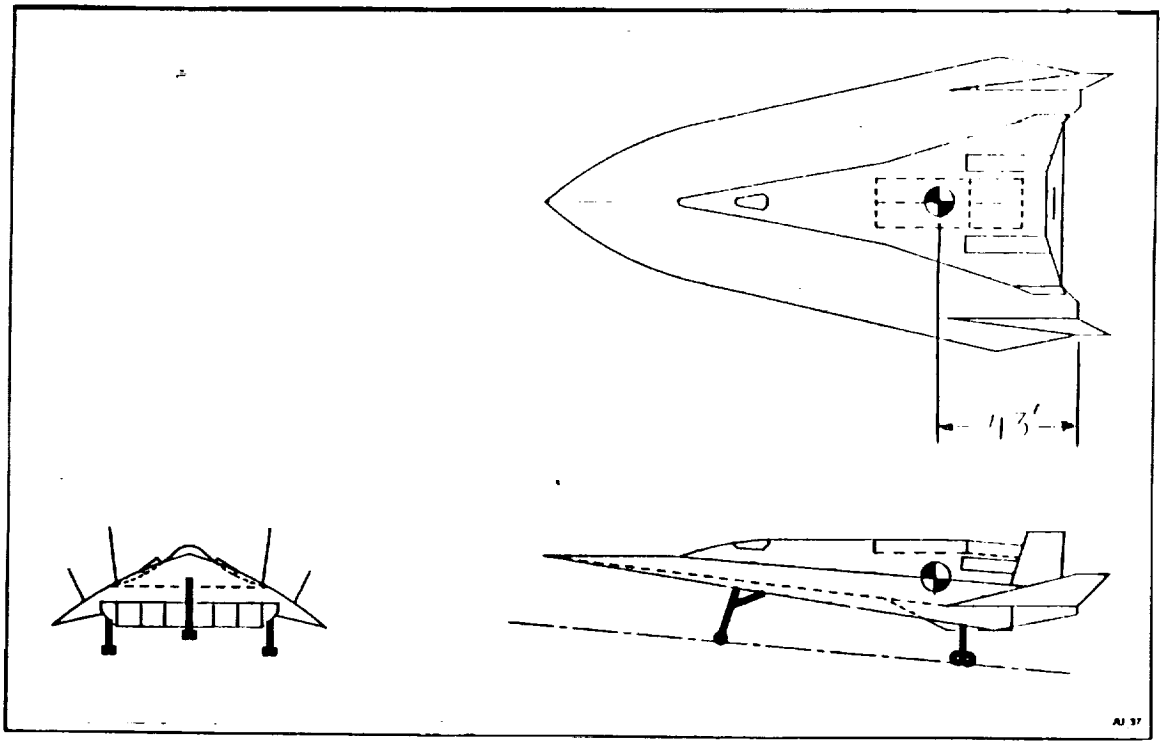

Figure 2.1. Proposed Waverider Two-Stage to Orbit Configuration.

learned winter quarter. The new carrier design, as shown in Figure 2.2, is much more controllable, has more volume, and has better performance than the waverider for the mission profile. The canards are included for increased control at staging and at takeoff and landing.

The aerodynamic analysis for the carrier was a difficult task. For the waverider, Polyhamus theory was used for subsonic, shock-expansion was used for supersonic, and modified Newtonian was used for hypersonic. For the new carrier, experimental data for a similar configuration was utilized by subtracting its skin friction, adding our skin friction, adding drag for our orbiter and interference, and scaling the wings and vertical tails in order to get C_L vs C_D curves for the entire Mach number range of the carrier.

The propulsion choice for the carrier has been the same both quarters. We plan to use Hydrogen-fueled tandem turbofan-ramjets with two-dimensional mixed compression ramp inlets and two-dimensional converging-diverging nozzles for the carrier. The

expansion surface in our nozzle configuration has been made much smaller in order to reduce the thrust vector perpendicular to the flight path. The propulsion system has been sized by the trajectory team to give the minimum total propulsion system weight of fuel plus engines and supporting systems over the entire mission profile.

Determining the system weights was an iterative task requiring inputs from each of the design sections. Many of the weights were calculated using statistical methods based on a given takeoff weight and planform areas. The propulsion system weight was sized by the trajectory team for minimum total weight of fuel plus engines for the entire mission profile. The takeoff weight was then determined by iteration so that a given carrier size would have the required payload capacity remaining in order to carry the orbiter. Preliminary calculations have also been made to figure out the volume of the components, a preliminary layout has been completed, and center of gravities have been computed. These have been used to get preliminary static margins.

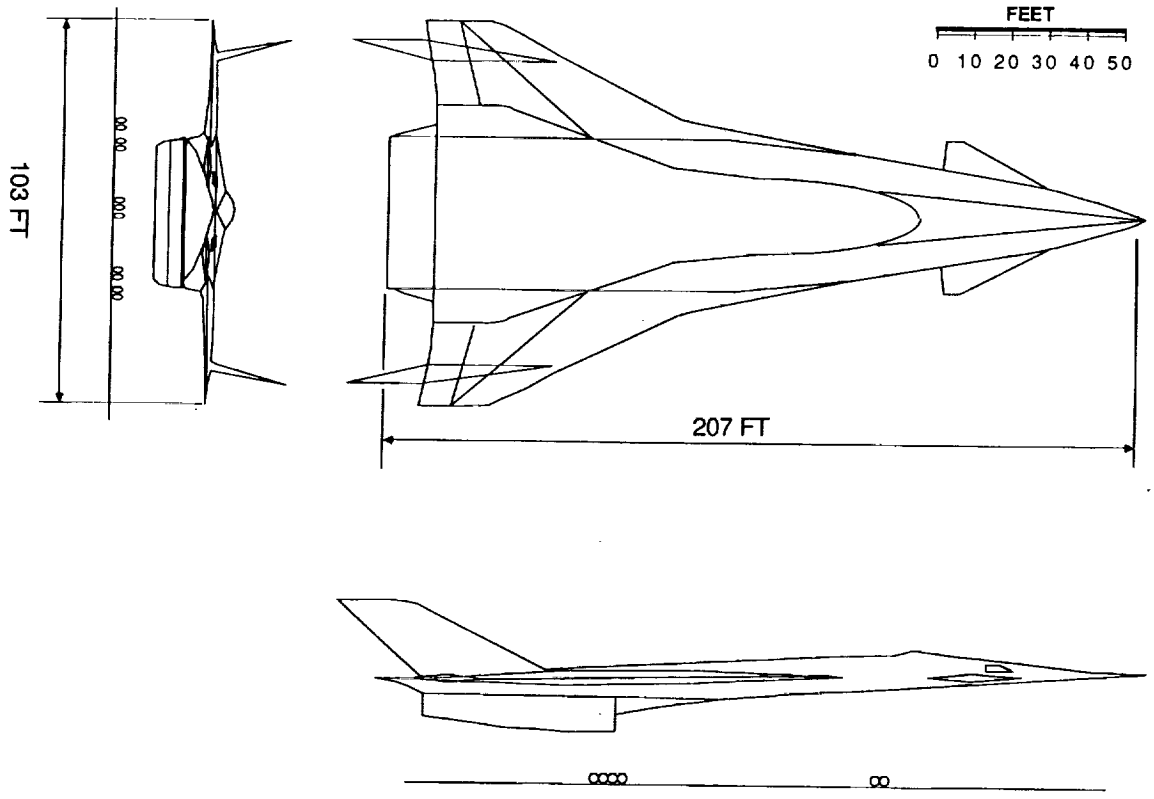

Figure 2.2. Proposed Carrier Configuration.

Aerodynamic heating becomes a problem for Mach numbers above 4. The short time the carrier spends above Mach 4 should allow us to get by with passive heat protection on the nose, wingtips,

canards, and vertical fins. Molybdenum-Nickel alloys have been proposed as the leading edge material in these areas.

Much work remains to be done on the carrier. A wind tunnel model is near completion, and can be used to analyze the subsonic aerodynamics. A more complete aerodynamic analysis is also in order. The static margin needs to be adjusted to make us less stable and to reduce our trim drag. Following this, a complete stability and control analysis needs to be completed.

The Orbiter design is similar in nature to many other hypersonic vehicle designs. It uses its narrow fuselage and blended delta wing configuration to produce a lifting body design. This design was picked because of the relatively high L/D that was produced.

The dry weight estimation was done using statistical methods. These weight estimations were the starting blocks for trajectory work and were constantly being reevaluated when new information was discovered. Once a dry weight for the orbiter was estimated, a propulsion system had to be analyzed.

The Orbiter researched two propulsion systems in order to find the best propulsion unit to minimize the Orbiter's weight. The two systems looked at were the rocket-only system and the scramjet/rocket system.

Upon doing trajectory analysis using ENTRAN, the results showed that the scramjet/rocket system would save about 63,000 lbs of fuel. Once it was decided that the scramjet/rocket system would be used, a staging point for scramjet to rocket had to be determined.

Although we initially believed that using the scramjets to the highest possible Mach number would produce the best results, we found that this was not the case. The higher the Mach number that the Orbiter reached before turning on the rockets, the more difficult it became. This is because of the increased liquid hydrogen required, as well as a larger thermal protection system. Thus, the Orbiter decided to turn on its rocket at Mach 12.3. This produced an orbiter staging weight of 317,000 lbs.

Both passive and active cooling systems were chosen for the orbiter. The primary concerns for the orbiter was reentry, but the use of scramjets in the atmosphere requires thermal protection as well. Lower Mach numbers for firing the rockets produces less heating in the atmosphere, and would simplify the system somewhat. The proposed thermal protection systems include spray cooling for the nose, indirect cooling for the leading edge of the wings and fins, and thermal shields (carbon-carbon with silicon covering) for the lower surfaces. The thermal protection system (TPS) weight was much lower for starting the rockets at

Mach 12.3 than at Mach 15.5.

The final proposed design of the orbiter employs a scramjet/rocket system to be staged at Mach 6-6.5 and 90,000 ft. The orbiter will then accelerate up to Mach 12.3 at about 120,000 ft, where its 1/2 SSME engine will be fired in order to reach the final velocity of 25,400 ft/sec required for a 300 mile orbit.

The final proposed configuration for the two stage to orbit system is shown in figure 2.3.

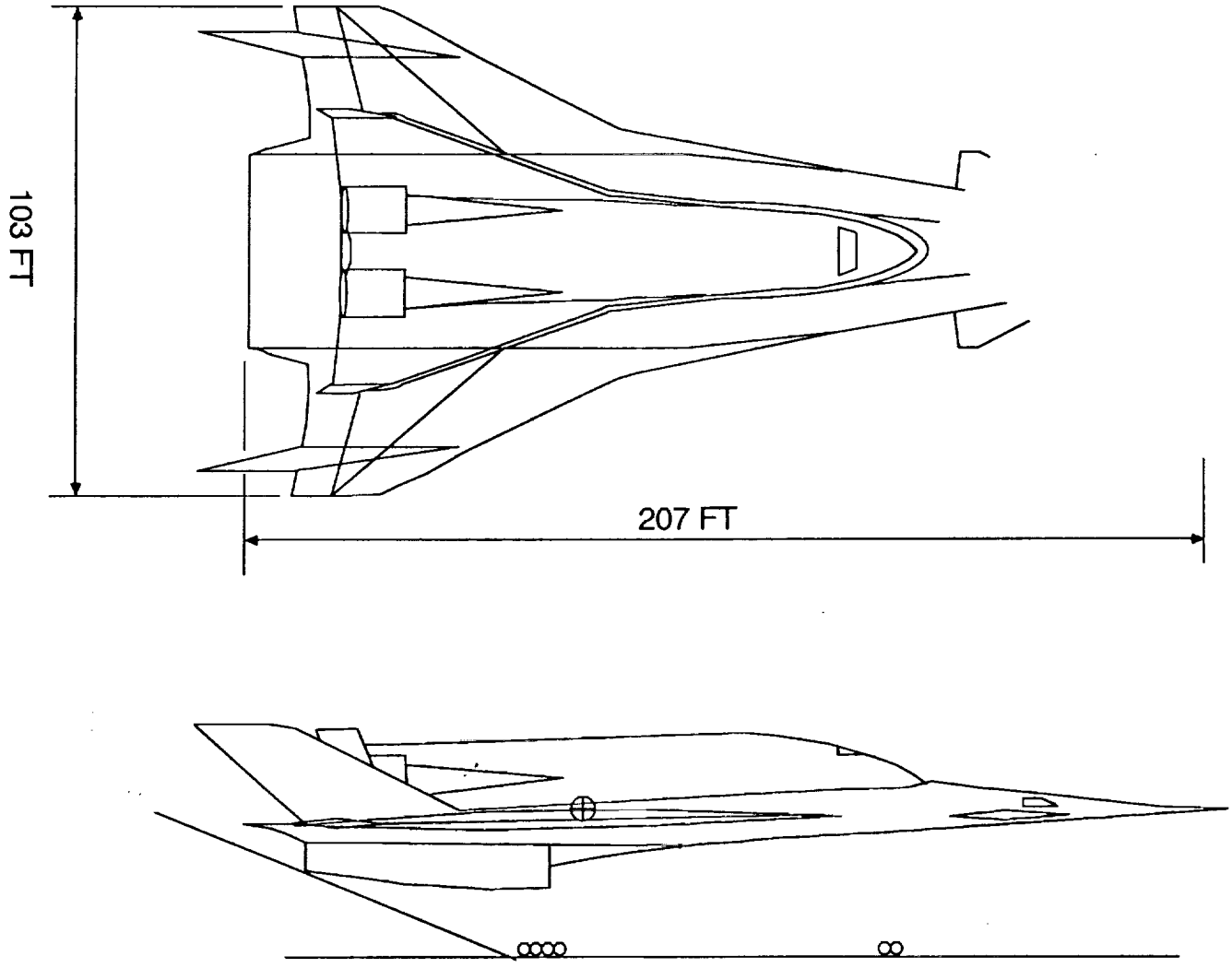

Figure 2.3. Proposed Two Stage to Orbit System Configuration.

Specifications

2-Stage to Orbit

Staging Mach #.....6-6.5
Staging Altitude.....90,000 ft
Takeoff Weight.....710,000 lb
  Carrier.....390,000 lb
  Orbiter.....320,000 lb

Carrier

Length.....207 ft
Height.....12 ft
Span.....103 ft
Wing Reference Area.....6800 ft^2
Aspect Ratio.....1.46
Wing Sweep.....70 deg
Propulsion.....6 Tandem Turbofan-ramjets
  90,747 lb Thrust ea. @ Sea Level

Orbiter

Length.....130.0 ft
Height..... 15.0 ft
Span..... 61.24 ft
Planform Area.....6,523.0 ft
Aspect Ratio.....1.46
Wing Sweep.....70 deg.
Propulsion.....8 Scramjets +
  1/2 SSME Engine

3. Mission Profile

The proposed mission profile begins and ends in either Texas or Cape Canaveral Florida. The carrier will take off under its own power in approximately 13,450 feet and begin its initial climb. An efficient path will be followed through the transonic region in order to reach a constant dynamic pressure ascent at 1500 lb/ft^2. This transonic trajectory deserves careful analysis, as any improvement can drastically cut our required fuel. A decrease in L/D of .2 at our transonic thrust pinch can as much as double the amount of fuel needed for a mission.

The constant Q trajectory is followed up to a maximum pre-staging altitude of 95,000 ft. where the carrier begins a shallow dive and the orbiter starts its engines. The carrier will be between Mach 6 and Mach 6.5 at the staging point of 90,000 ft., where the orbiter will be lifted off and allowed to proceed under its own power. The carrier will turn off its engines and put out spoilers in order to increase drag, slow the carrier down, and put distance between the carrier and the orbiter.

The Orbiter will stage at Mach 6.5 at an altitude of 95,000 ft. From this point the Orbiter will travel at this altitude until it reaches a Q of 1500 lb/ft^2. It will then follow a constant Q trajectory at 1500 until it reaches a Mach number of 12.3 where the rocket system will take over. The rocket will burn for approximately 3 to 4 minutes until the delta v fulfills our mission requirements.

The reentry trajectory will be similar to that of the Space Shuttle. We will turn the Orbiter around and fire the SSME engine for a short duration to slow ourselves down, slow enough to reach reentry velocity. The Orbiter will be coming in the atmosphere at a relatively high angle of attack to slow itself down. The reentry will be unpowered descent, landing at Kennedy Space Center or another available runway.

After staging the orbiter, the carrier will perform a powerless pull-up maneuver in order to reduce heating and in order to slow and turn. The carrier will then turn and head home, never exceeding a load factor of 5 g's. The returning glide will terminate when either the altitude is getting too low and the engines are required, or when the carrier reaches the altitude where the subsonic maximum L/D for the carrier weight is achieved for the cruise home. The trajectory of the carrier is covered in more detail in Chapter 4.1. Figure 3.1 shows an exemplary flight path of the carrier for the entire mission.

Figure 4.1. Altitude vs. Downrange.

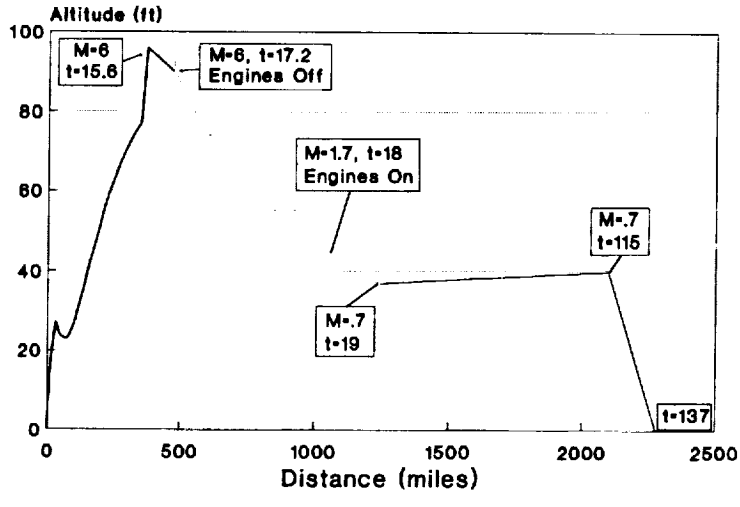

4. Carrier Design

The design of the carrier was a very difficult task. Each aspect of the design is dependent on every other aspect of the design. Preliminary research was used to make initial assumptions which could be used to start the design, beginning with trajectory analysis.

4.1. Trajectory - Carrier

The carrier's trajectory analysis is a highly nonlinear multi-variable optimization problem. The task is much too complex for analytical methods. A systematic means of iteration was used to optimize the trajectory. Whenever possible, parameters were combined to reduce the complexity of the problem. Preliminary research, estimations, and crude models were used to find initial guesses with which to begin the iteration and analysis.

The analysis was divided into three phases: an ascent phase, a staging phase, and a descent and return phase.

4.1.1. Ascent

The goal of the ascent phase is to take the orbiter to the staging conditions while keeping the takeoff weight to a minimum. From an engine/performance point of view, a trajectory with a high Q (dynamic pressure) is desirable since the engines operate best at high Q values. Unfortunately, the maximum Q value to which the carrier can be exposed must be limited, due to structural and aerodynamic heating limitations. A maximum Q of 1500 (lbs/ft^2) was selected based on research of similar applications and material properties.

Once a maximum value of Q was set, most of the ascent phase could be flown on this constant Q line. However, lower dynamic pressures were necessary for staging, takeoff, and transonic flight. For these regions, the trajectory breaks away from the constant Q line at the beginning and end of the ascent phase as shown in Figure 4.1.1.

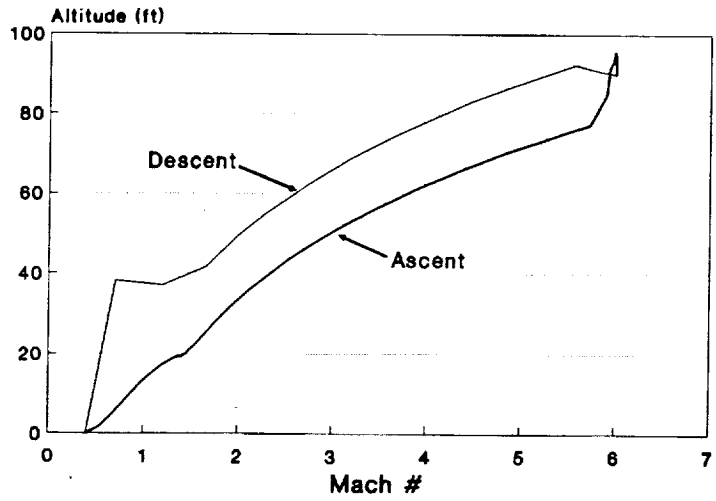

Figure 4.1.1. Altitude vs. Mach Number (Q=1500)

To get from the takeoff condition to the Q line, the carrier must pass through the transonic region. This is where the carrier's thrust pinch occurs. Passing through this thrust pinch while minimizing takeoff weight became one of the most important parts of the trajectory design. The Q at which the carrier passes through the transonic region has a great effect on the thrust pinch and takeoff weight. The thrust pinch resulting from the carrier's finalized ascent trajectory is illustrated in Figure 4.1.2.

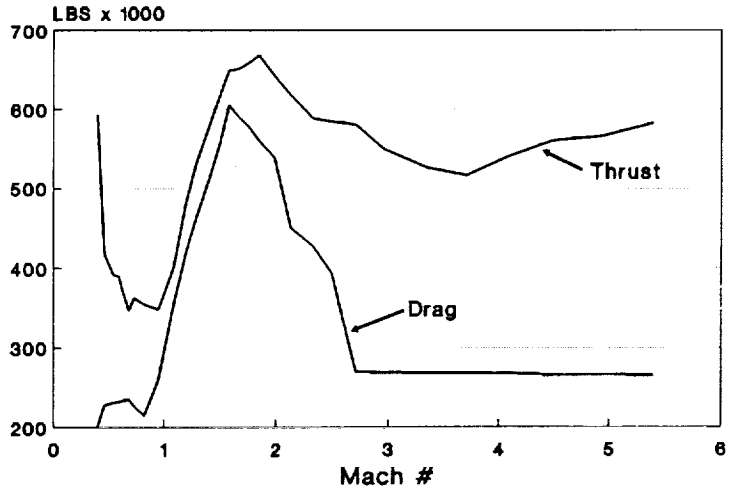

Figure 4.1.2. Thrust Pinch

Finding the optimal trajectory through the transonic region is a difficult task. Energy methods may be the best method, but they are extremely tedious and difficult to fly, and may be approximated by trial and error on simpler flight paths. In addition, some important general trends can be inferred from the study of other optimum trajectories. Arbitrary paths through the transonic region gave the initial guesses to begin the iteration process. After studying the results of the iteration process, it was found that if the Q value was too low, the thrust pinch occurred around Mach 1.2, whereas, higher Q values caused a thrust pinch around Mach 1.4. This helped in honing in on an optimal transonic trajectory, which yielded the elongated, drawn-out thrust pinch shown in Figure 4.1.2.

4.1.2. Staging

During the staging phase, the carrier must maintain the orbiter at the staging conditions. Determining the optimal staging conditions was an iterative process involving the design of the orbiter as well as the carrier. The orbiter's weight decreases a great deal as the staging Mach number increases, so the highest Mach number achievable without requiring additional propulsion systems was desired. This Mach number should be between Mach 6 and Mach 6.5. At these high Mach numbers, it was necessary to go to an altitude of at least 90,000 feet to reduce the Q and alleviate structural and aerodynamic heating problems. By keeping the staging altitude below 95,000 feet, we made more efficient use of the scramjets on the orbiter.

A slightly negative angle of attack and flight path angle were desired during the staging phase. This gives the carrier a nose-down pitching moment, which will be needed to counteract the weight loss at separation. The negative angle of attack also prevents nose vortices from interfering with the separation process. To achieve these criteria, the carrier begins its staging phase at Mach 6, 95,000 feet. The staging should be accomplished over a period of 90 seconds.

4.1.3 Descent

The goal of the descent phase is to cool off, turn around, and return to the launch site, while using as little fuel as possible. The quickest way to cool off after staging is to shut off the engines and climb. By doing this, we decrease Mach number and increase altitude. Both serve to decrease Q and alleviate the heating situation. Once a sufficiently low Q is reached, the carrier begins its descent and turn along this Q line. The flight path angle is set for this given Q and the turning radius then is defined such that the carrier experiences the maximum allowable N (number of g's). This turning radius

changes as the flight path angle changes, since both the pull-down and turn maneuver affect N.

This glide-and-turn descent is continued until the cruising point is approached. Then, two of the engines are turned on and a slight pull-up begins so that the carrier does not overshoot its cruise point. Once the engines are on and the flight path begins to level out, the turn can become tighter. At the completion of the turn, the cruise point is reached and a straight return and landing follow.

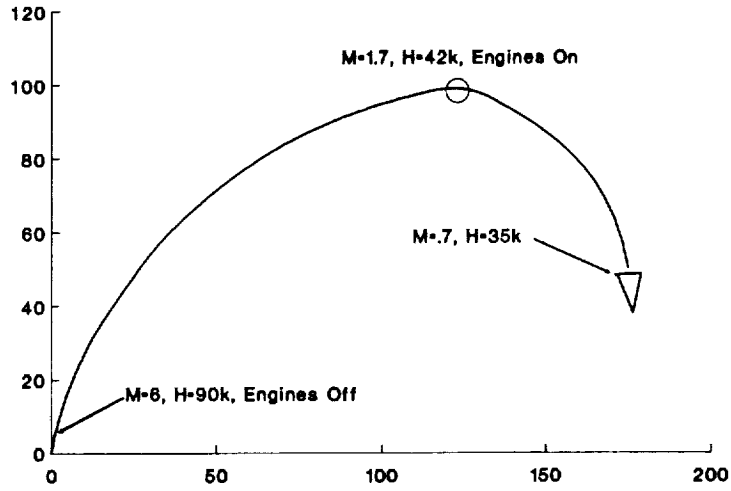

Figure 4.1.3. Turn Profile

4.1.4 Abort

Precautions for an aborted mission were taken into consideration in the design of the carrier and its trajectory. A launch site in Texas would put the hypersonic flight path over the Gulf of Mexico, allowing several abort options. Not only could the carrier turn around and return to base, but it could land at a point along the northern gulf coast or in Florida. This would reduce the time before landing and remove the need for a long 180 degree turn.

Figure 4.1.4. Carrier Path

4.2. Propulsion

4.2.1. Engine Selection

Several things had to be considered when deciding the best type of engine for this aircraft. The most important factor in engine selection was the mission profile. The engines must be able to operate efficiently over the entire range of velocities and altitudes required for the mission. Other important factors include overall propulsion system weight, fuel efficiency, drag, and ease of integration into the overall system.

The most important driver in the above criteria is the velocity profile, which is supplied by the trajectory team. Because the aircraft will be operating up to a Mach Number of 6, the propulsion system must be able to provide sufficient thrust to accelerate the aircraft to this speed. Initially, augmented turbofan engines were studied; however, these engines can only operate up to Mach 3. The next type of engines to be studied were of the ramjet class. These included scramjets as well as ramjets, although more data was available on the ramjets. It was determined that scramjets just begin to become efficient around Mach 6, which is only obtained at the very end of our acceleration. For this reason, scramjets were ruled out for a means of propulsion for the carrier. This left us with the ramjet. The problem with ramjets is that they cannot operate efficiently until around Mach 3, so another means of propulsion is necessary to accelerate to this point. The solution came in the form of a mixed engine type called a turbofan-ramjet. This system consists of an augmented turbofan engine in the same package as a ramjet. The turbofan operates up to a given airspeed at which the ramjet takes over for acceleration to higher Mach numbers.

There are several different ways of combining turbofan and ramjet engines. The three combinations considered for this study were over/under, wrap-around, and tandem configurations. The performance of all three configurations is comparable. The first and most obvious difference, as shown in Figure 4.2.1, is the size and shape of the various options. The tandem TFR tends to be long and slender, whereas the wrap-around and over/under TFR's are much shorter and wider. The size of the engine does become an important factor due to the rather lengthy inlets that must be appended to these engines in order to control the engine airflow rates at high Mach numbers. For our carrier, a tandem configuration was selected since, even after appending an inlet and nozzle, engine length was not a problem.

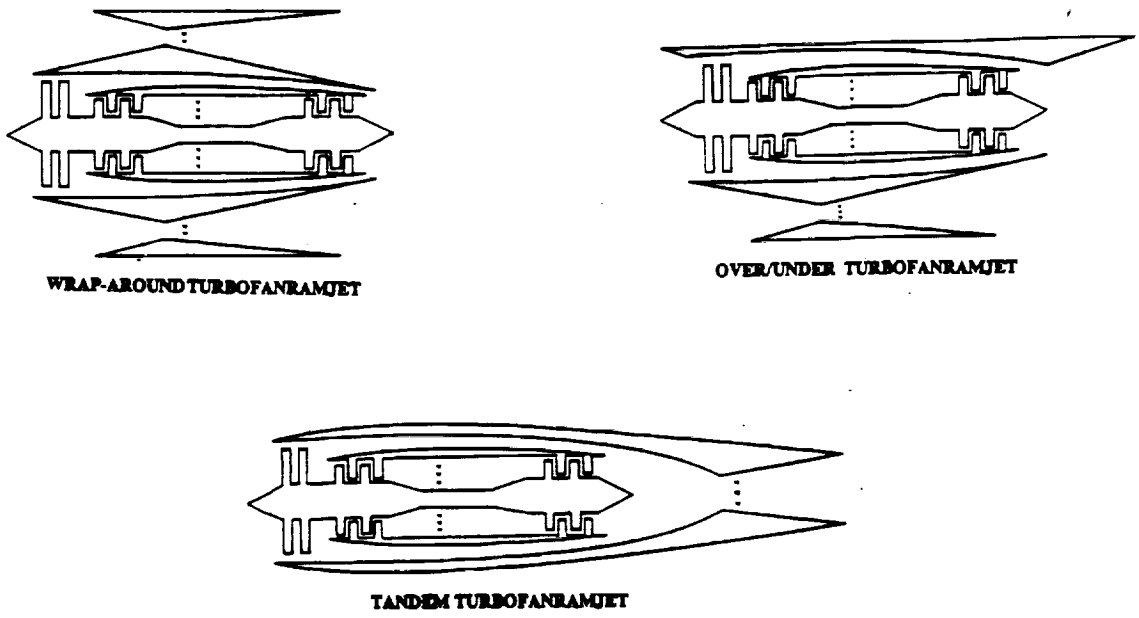

Figure 4.2.1. Turbofan-ramjet Configurations.

4.2.2. Fuel Selection

Once the turbofan-ramjet (TFR) engine had been selected, we were charged with the task of finding a suitable fuel to power these engines. Two fuels, methane and hydrogen, are available to power the TFR engines. Hydrogen has a high energy per unit mass, but its low density gives it a low energy per unit volume. Thus, the TFR engine powered by hydrogen has a significantly lower specific fuel consumption than the one powered by methane, but the volume of fuel burned is much higher. One justification for the higher volume is the utility of hydrogen for an aircraft cooling system. Hydrogen must be kept at a very low temperature in order to keep it in its liquid state. Therefore, the fuel could possibly be used in the active cooling of the aircraft, providing that a system is devised that will keep the hydrogen under enough pressure to maintain the liquid state. In addition, Methane is a very unsafe propellent. If a fuel leak is present, methane is more dense than air and it stays just above the ground presenting a fire hazard, whereas hydrogen is so light that it quickly dissipates into the atmosphere.

4.2.3. Performance of the Turbofan-ramjet

The thrust available at a given Mach number for the hydrogen-fueled TFR engine is a strong function of altitude, making mission profile optimization very important. As the altitude and

Mach number increase, the rated thrust will decrease significantly. According to data collected, the most efficient operating envelope of these engines is at altitudes between 60,000 and 80,000 feet for Mach numbers between 2.5 and 6. However, the maximum Q limitations on the carrier limit it to a somewhat lower thrust than would be possible at a much higher Q, though the thrust at a Q of 1500 is sufficient to get the system to staging at Mach 6 and 95000 ft.

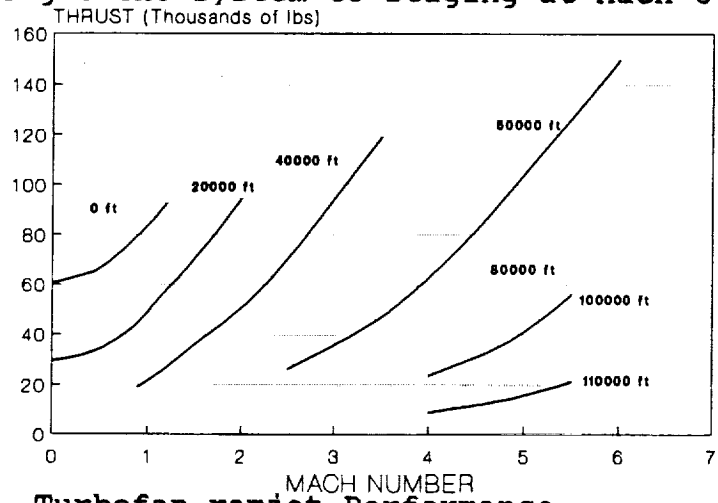

Figure 4.2.2. Turbofan-ramjet Performance

4.2.4. Turbofan-ramjet inlets

One of the most important factors in utilizing the TFR engines is supplying them with the correct airflow that they require at each point in the trajectory. In order to supply air to both of the engine cycles, the flow must be slowed down to subsonic speeds. There are several inlet designs commonly used that will accomplish this.

The first type that was looked at was the internal compression inlets. In internal compression inlets, all compression takes place inside the inlet duct and the throat is inside the duct. Internal compression ducts involve an decrease in area before the subsonic diffuser. These inlets are very sensitive to the pressure behind the normal shock, and often encounter unstarting if the back pressure forces the shock outside of the duct.

Another type of inlet that was studied was the external compression inlet. External inlets utilize a ramp system to turn and compress the flow. These ramps are located outside of the diffuser, hence the name external compression. External compression inlets are not as sensitive to unstarting because the back pressure can be regulated by use of bleed ducts that divert air away from the diffuser duct.

The final type of inlet that was looked at was a compromise of the two previously mentioned. This inlet type is called a mixed

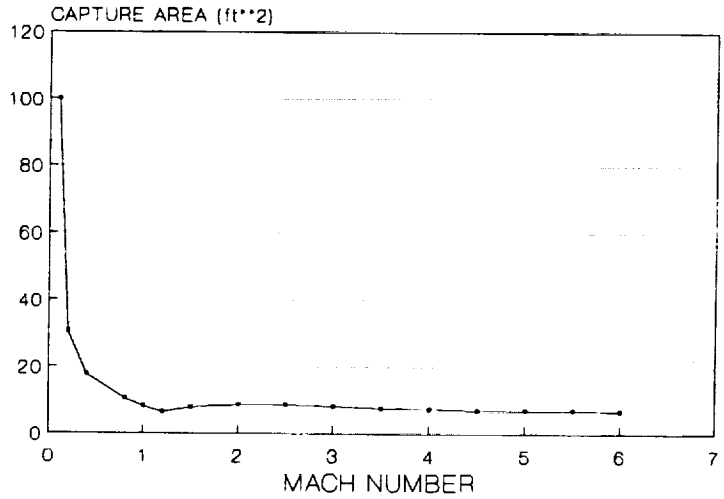

Figure 4.2.3. Required Capture Area.

compression inlet. These inlets utilize the better points of both internal and external compression inlets into one very efficient design. The external ramp geometry is variable so that the oblique shocks can be focused close to the cowl lip. Doing this produces the good pressure recovery that is required for efficient engine operation. This type of inlet was found to be very efficient, and was the type selected for this project.

Once the inlet type was decided, the next step was to determine what the ramp angles needed to be. To do this, it was determined that there were various critical areas of the flight that the thrust levels given in the General Electric data had to be met. These critical areas were at Mach 1.4, 4 and 6. At Mach 1.4, the drag produced by the aircraft was very close to the thrust produced by the engines, which is called the thrust pinch. It was determined that the aircraft could indeed accelerate through this region, but the thrust had to be equal to the levels indicated by the data. Mach 4 is a critical point because of the fact that this is the point where the normal shock is completely inside the diffuser duct, and the inlet must be designed accordingly. The final design point was at Mach 6, as this was our maximum speed and again, the inlets were required to deliver an acceptable pressure recovery for the engines to operate correctly.

The way that the ramp angles were determined was basically through trial-and-error. Various configurations were tried, and the pressure recovery determined through the use of Shock-Expansion theory. If the pressure recovery was at an acceptable level, then the geometry of the ramps was calculated to see if the ramps would fit onto the aircraft. this was done time and time again until finally a design was found that would work for all three critical

areas of the flight. These ramp angles are shown in Figure 4.2.4.

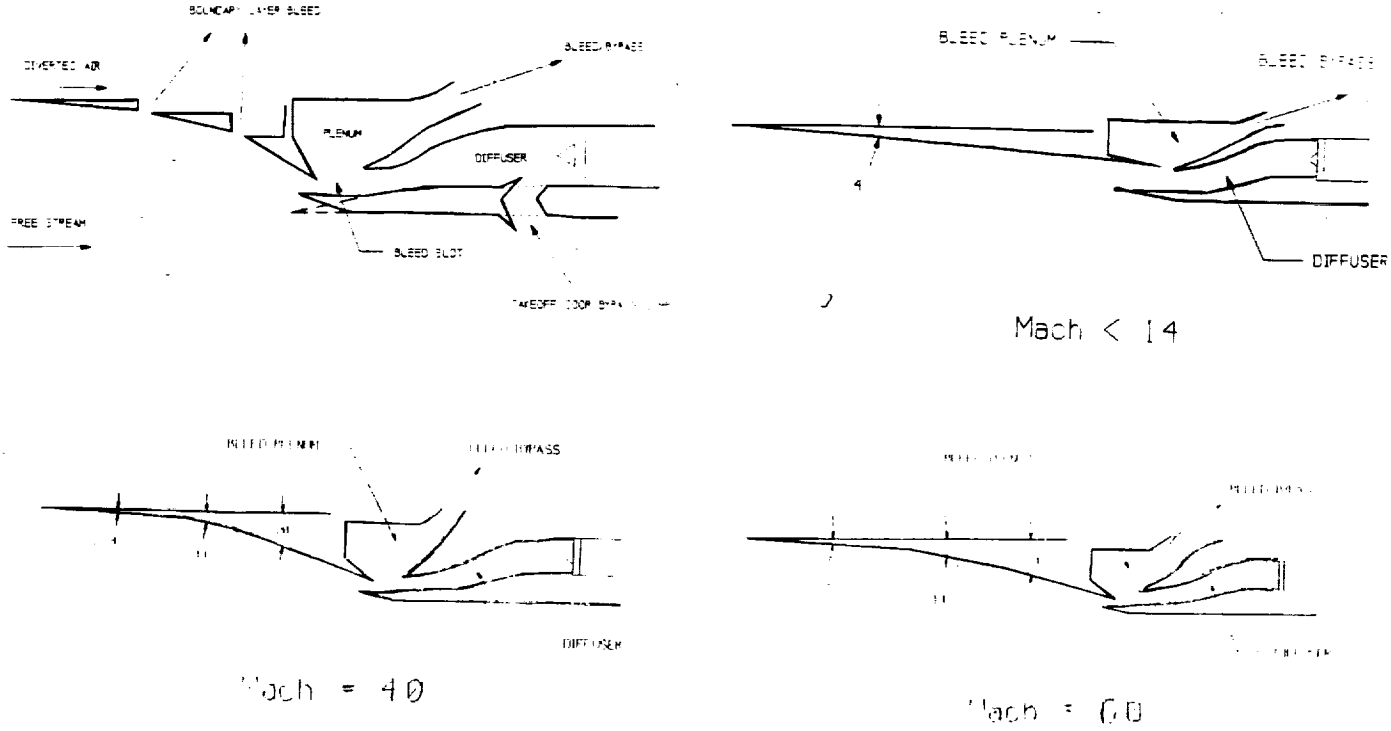

Figure 4.2.4. Inlet Ramp Angles.

4.2.5 Nozzles

The exhaust nozzle plays an important role in developing the propulsion system to its fullest potential. The purpose of the exhaust system is to utilize as much of the engine's energy as possible to produce thrust, working within the restraints of size and weight. This is achieved by expanding and re-directing the flow. Unfortunately, when travelling at high Mach numbers, it is not practical to fully expand the flow. Very large nozzle area ratios are required to fully expand engine exhaust, and size and weight restraints prohibit the use of such large nozzles in most practical cases.

Since the flow cannot be fully expanded, the nozzle must be designed to expand the flow as much as possible, and, more importantly, redirect the flow so that the component of flow perpendicular to the thrust force is minimized. A variable geometry nozzle is necessary to expand the flow over the wide range of flight Mach numbers encountered. Several variable geometry configurations were considered. In general, two-dimensional configurations were able to provide a greater range of area ratios with smaller associated weight penalties than axisymmetric configurations. For this reason, axisymmetric nozzles were quickly ruled out.

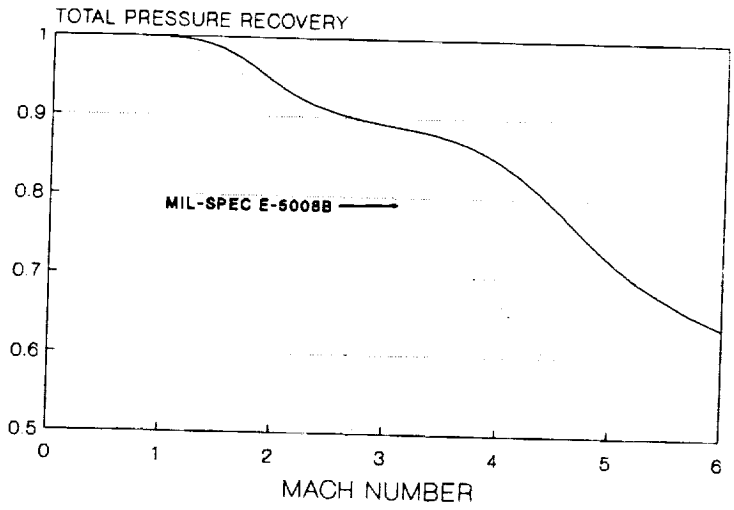

Figure 4.2.5. Recovery Pressure

Two different types of 2-D nozzles were considered. Variable geometry converging-diverging nozzles seemed to provide a viable option. These incorporate four movable ramps which form a converging-diverging nozzle as shown in Figure 4.2.6. A Sern nozzle also provided an attractive option because it uses the lower aft surface of the carrier to expand the exhaust flow. By doing this, the nozzle weight is significantly reduced and the base drag of the carrier is also reduced. Because of these last two considerations, the Sern nozzle was seen to be the most promising. However, the benefits of having variable geometry could not be overlooked, so a nozzle was developed that utilized the good points of both types. The bottom of the carrier was used as an expansion surface, while a variable geometry ramp was used as the lower expansion surface. This enabled us to control the direction of the expanded flow as well as regulate the base drag that is encountered. A picture of the nozzle design can be seen in Figure 4.2.7.

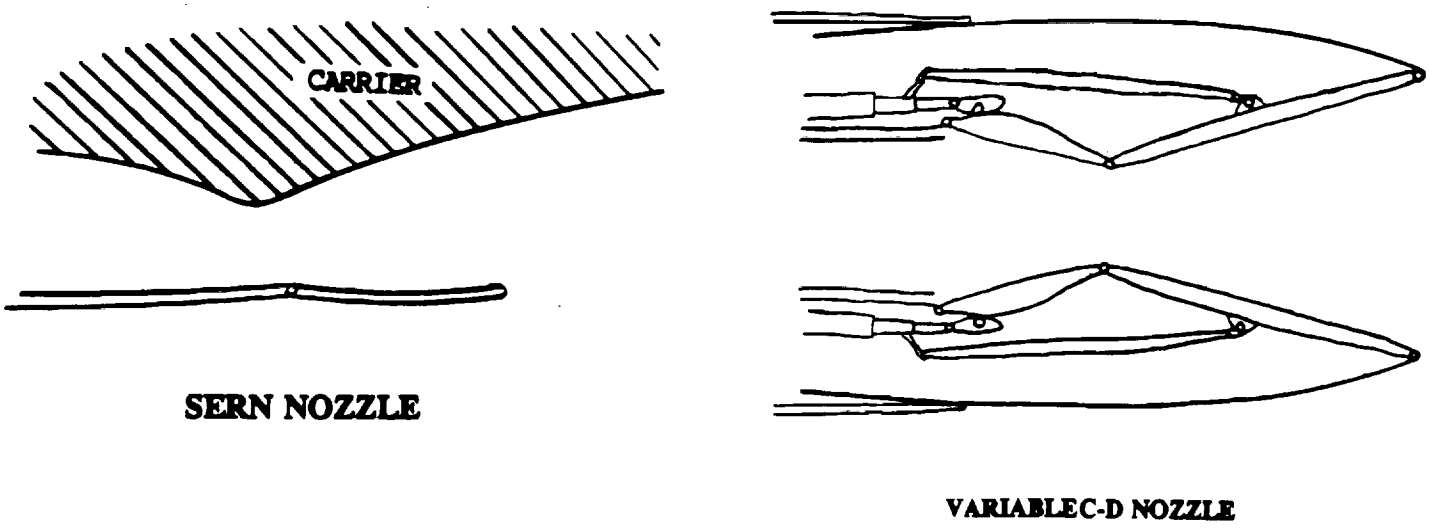

Figure 4.2.6. Nozzle Configurations.

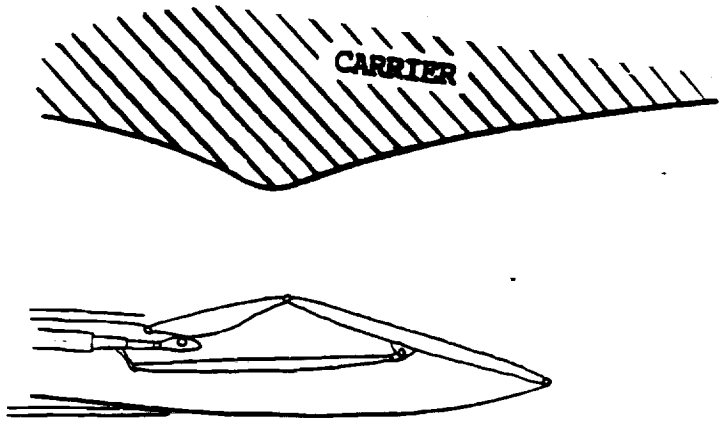

Figure 4.2.7. Nozzle Design

4.3. Aerodynamics

4.3.1. Subsonic Aerodynamics

Subsonic Aerodynamic data was obtained by modifying experimental data from reference 1 to take into account our skin friction in comparison to the wind tunnel model's skin friction. This data was used in conjunction with the transonic and supersonic data to construct the drag polar in Figure 4.3.1.

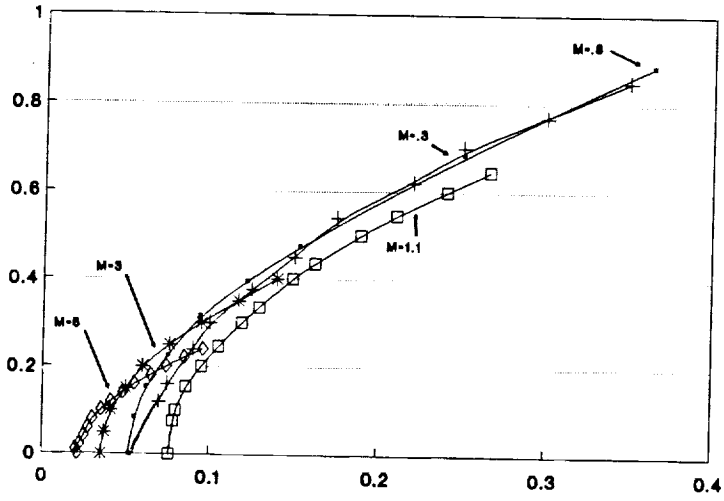

Figure 4.3-1: Drag Polar

4.3.2. Transonic, Aerodynamics

Transonic aerodynamics were determined using modified experimental data from similar double-delta configurations (Reference 2). The skin friction for the model was removed, the skin friction for us was added, and drag was added for the Orbiter and for interference. The data was provided for Mach .8, .9, .95, .98, 1.1, and 1.2.

4.3.3. Supersonic Aerodynamics

Shock expansion theory provided approximate results for analyzing a waverider design at supersonic speeds. These numbers were used for the preliminary analysis of the trajectory of the new configuration. Finally, modified experimental data was used (references 3 and 4) to get drag polars for Mach 2, 2.36, 2.86, and 6. These drag polars were interpolated for calculating L/D's throughout the trajectory.

4.4. Heat Transfer

4.4.1. Temperature Prediction

The extreme surface temperatures encountered due to aerodynamic heating at high Mach numbers are of major concern in the design of supersonic and hypersonic vehicles. Stagnation regions such as those at the nose and leading edges experience the highest temperatures and thus were the focus of our initial investigation.

The major obstacle in predicting surface temperatures experienced during the ascent of the carrier to staging altitude and Mach number was determining the heat transfer coefficient, h. This parameter is a function not only of flowfield properties such as pressure, density, and Mach number but also of geometric constraints including angle of attack, radius of curvature, and whether the flow is 2-D or axisymmetric. Semi-empirical equations developed in a Conceptual Design Aerodynamic Heating Analysis (CDHEAT) were employed to determine the heat transfer coefficient for the leading edges of the delta wings. To determine surface temperatures at the nose stagnation region a purely theoretical approach was taken in order to determine temperatures from takeoff to stage (Ref. 5).

For our initial investigation of the effects of aerodynamic heating on the nose and leading edge regions, a calorically perfect gas with a gamma of 1.4 was assumed. This yielded artificially high skin temperatures for boundary layer temperatures of ≈1000 °F and higher because at these temperatures gamma becomes a function of temperature and decreases in value. A "factor of safety" measure was also taken by assuming an entirely turbulent boundary layer in the nose and leading edge regions. Truitt (Ref. 5) justifies the turbulent boundary layer assumption in saying "...the boundary layer in the stagnation region may become turbulent even at low Mach numbers....produced by either roughness of external disturbances which are amplified as they enter the boundary layer region." In determining the heat transfer coefficients, the nose and leading edges were analyzed as isolated bodies, and therefore the effects of boundary layer interactions, interference, and viscous interactions were not considered.

The variables involved in the analysis of the skin temperatures are not constant but vary with the trajectory of the carrier. We were therefore forced to deal with the time dependency of these variables and were unable to say that the amount of heat imparted to the structure is exactly balanced by the radiative heat transfer away from the structure. Also, because of time dependency, the surface temperatures become a function of the skin material. This is manifested in the heat absorption capacity of the skin, G, and is a function of skin thickness, specific heat, and density. To determine an initial value of G, conservative values of thickness,

specific heat, and density were chosen to maintain a factor of safety in the analysis. The governing equation for the heat-transfer process is thus given by (Ref. 5):

$$\frac{d}{dt}(T_w) = \frac{1}{G} \times [h(T_{aw} - T_w) - \epsilon \sigma T_w^4]$$

This equation was solved by employing a Runge-Kutta routine with Mach number, pressure, temperature, density, and heat transfer coefficients as functions of time. As mentioned earlier, gamma was taken to be constant as was the Prandtl number. The methodology used in the development of the program is outlined in Appendix A.

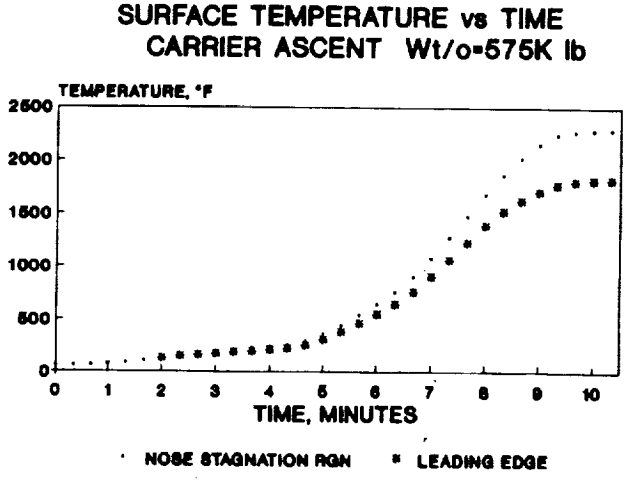

Figure 4.4.1. Temperature vs Time

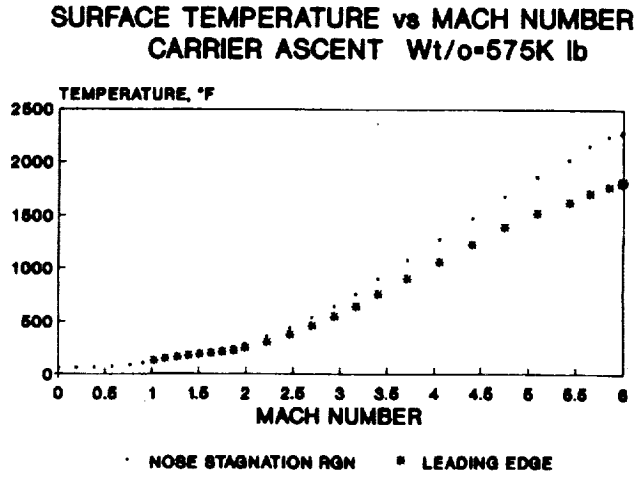

Figure 4.4.2. Temperature vs Mach #

Figures 4.4.1. and 4.4.2. show the results of the stagnation region skin temperature analysis. The time over which the surface temperatures were evaluated includes a 1 minute cruise at staging Mach number and altitude to take into account the time needed for the orbiter to stage. It can be seen from Figure 4.4.1 that during the 1 minute cruise the skin temperatures indeed begin to level off to steady state values, and these values correspond very closely to temperatures determined in a preliminary steady state analysis. It can also be seen from the graphs that the nose stagnation region experiences considerably higher surface temperatures than the

leading edges as the Mach number becomes higher. This is to be expected since in the vicinity of the nose the flow is 3-D in nature as opposed to 2-D along the leading edges; the 3-D "relieving effects" experienced in the nose region cause the boundary layer thickness to be smaller and the corresponding temperature gradients and surface temperatures to be larger than those for the leading edge.

4.4.2. Materials

From the surface temperature analysis it was concluded that typical aircraft materials would not be able to withstand the aerodynamic heating present during the flight of the carrier. To withstand such intense thermal loading, the materials employed at the nose and leading edges must maintain their strength at elevated temperatures but also be ductile enough to form easily and resist brittle fracture. Unfortunately, materials with the highest melting temperatures and strong creep resistance properties are also those materials that possess little to no impact strength and are brittle in nature. Other properties such as a low coefficient of thermal expansion to minimize thermal stresses, high thermal conductivity, and high emissivity are also advantageous in high temperature materials.

Several types of materials were considered for use at the nose and leading edges of the carrier. Carbon composites possess high melting temperatures and good thermal properties at the temperatures to be encountered, but carbon oxidizes very easily at high temperatures and would need to be replaced after every flight. Non-metallic refractory metals also have extremely high melting temperatures, but as discussed earlier, these types of materials have a very low ductility and practically no impact strength. Cermets, a combination of ceramics and metals, are an attempt to combine the ductility of a metal with the heat resistance of a ceramic, but even these materials cannot attain the necessary levels of strength and heat resistivity for use on high speed aircraft.

Molybdenum, a refractory metal, possesses good structural integrity and excellent creep resistance up to ≈2000 °F but is very dense (4 times that of aluminum) and must be protected against oxidation at elevated temperatures. Fortunately oxidation can be eliminated by plating the molybdenum with nickel and subjecting the combination to heat treatment which bonds the two metals by diffusion. Because of the combination of strength and creep resistance of molybdenum and the high emissivity of the nickel coating (.89), we chose nickel bonded molybdenum as the material for the nose stagnation region, the wingtips, the canard leading edges, and the control surfaces' leading edges. Due to the short amount of time the nose stagnation region will be at temperatures in excess of 2000 °F (approx. 3 minutes), we feel that the nickel

molybdenum nose cone can survive over an extended number of flights without the aid of additional active/passive cooling mechanisms, instead of using the H_2 transpiration cooling proposed last quarter.

4.5. Weights and Balances

4.5.1. Weights

The weights of each component (figure 4.5.1.) were determined using a FORTRAN code based on fixed weights and statistical methods outlined by Nicolai and other sources, to be mentioned later. To

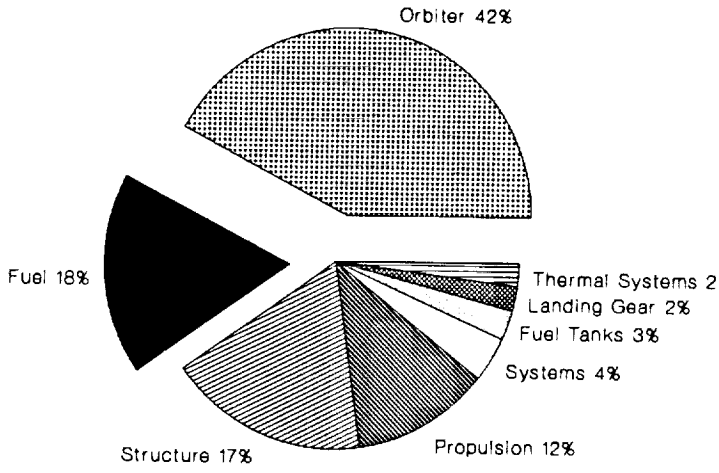

Figure 4.5.1. Weight Statement

determine the structure weight, the entire wing of the carrier was modeled as an Air Force fighter wing. Knowing the wing area, thickness to chord, and wing loading, the structural percentage was determined by the equation in Nicolai, and the result was multiplied by 1.64, the ratio of titanium weight to aluminum weight. The fuselage weight was determined in much the same way.

Propulsion needs and fuel weights were determined by the propulsion and trajectory teams, and each engine was assigned a weight of 6,100 lbs. To find the engine systems weight; ducts, inlets, pumps, etc, a formula provided by General Electric was used that estimated systems weight by the capture area per engine and the number of engines used.

The weights of the fuel tanks and CG control systems were determined using equations in Nicolai based on the amount of fuel used, and an additional 50% was added since we are using cryogenic fuel.

The landing gear used in the carrier is that used in a Boeing 747. The 747 uses two sets of rear landing gear, but only one was

decided for the carrier for several reasons. First, the 747 has a takeoff weight of 800,000 lbs, 95,000 heavier than the carrier. Secondly, since two thirds of the takeoff weight for the carrier is fuel and payload, the landing weight will be half that of a 747. Finally, the landing gear on a 747, for safety reasons, was designed to be able to withstand a fully loaded landing on only one set of wheels. For these reasons, and to save weight, only one set was used.

The "systems" weight refers to anything left out; fuel lines, control surfaces, valves, fasteners, etc.. The cockpit weighed in at 10,000 pounds, determined by the weight of the cockpit of a B-1 bomber, which is less than 2% of the takeoff weight. It was included in with systems.

4.5.2. Volume

To be sure that everything would fit and that there would be sufficient room for fuel, the cockpit, engines, and systems, the total volume was determined through simple geometric calculations to be 107,600 cubic feet including the wings. From this was subtracted the fuel volume (liquid hydrogen at 4.1 lbs/cubic foot for 150,000 lbs of fuel) and an extra 10% for tank bulk, the space taken up by the engines and their systems (supplied by propulsion), the nosewheel, cockpit, and buffer space for the passive heat transfer systems. Structure volume turned out to be small enough to be neglected.

After all the component volumes were subtracted it was discovered that over 30% of the total volume was empty space. To reduce the amount of this wasted space, the height of the craft was cut from 13.5 feet to 12 feet. This reduced the volume to 97,600 but still left us with nearly 20,000 cubic feet of unused volume. To partially rectify this, the wing tanks were removed and the amount of fuel space increased (the necessary fuel volume only took up 48% of the total space), which would allow for better versatility (Figure 4.5.2).

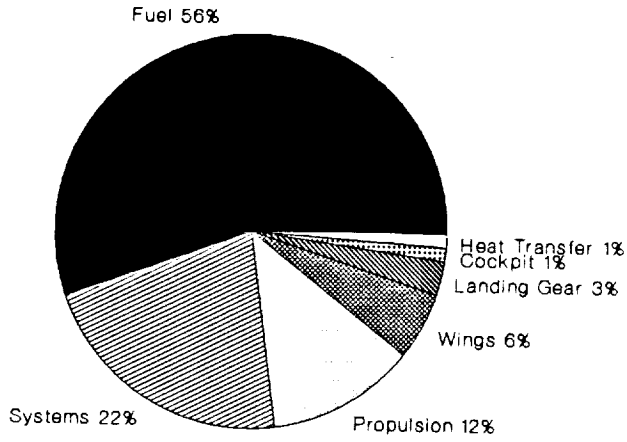

Figure 4.5.2. Volume Statement

For ease of entry and to allow for windows on the side of the carrier, the cockpit was placed as far forward as possible. At it's present location it is 26 feet from the nose and is 10 feet long, 9 feet wide, and 5 feet high.

4.5.3. Balances

To determine CG locations a FORTRAN code was written taking into account each individual component weight and CG location all along the carrier. The weights and positions were then massed together using simple mechanics to obtain the CG. The fuel tanks were partitioned along the width of the carrier (Figure 4.5.3) to allow for maximum control of CG location by draining tanks in a select order, also to avoid instability by fuel sloshing.

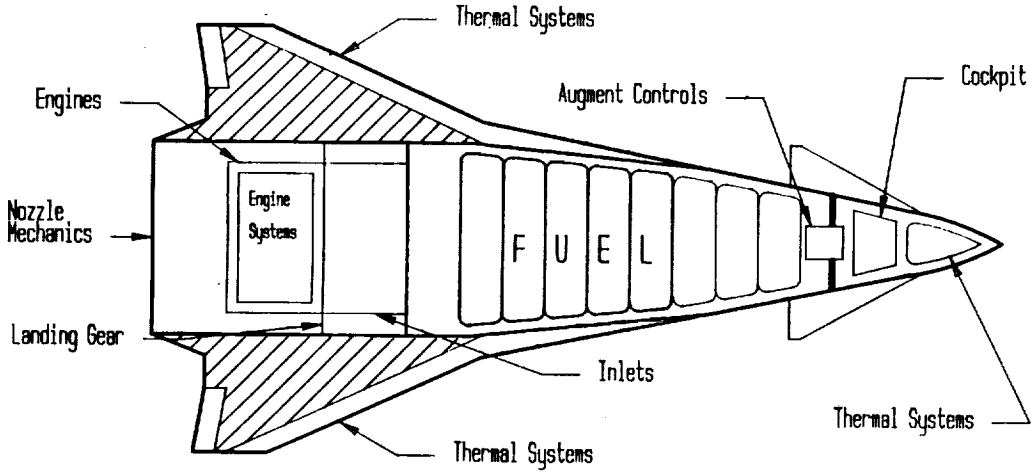

Figure 4.5.3. Schematic Layout

The tanks are depleted from back to front; the rear most tank is drained completely before the next one is tapped, which will keep the CG as far forward as possible throughout the flight. To determine the extent of CG travel, the two fore most tanks were assumed to be full at staging and then used in the return flight which produced CGs at the following critical locations:

	X-CG	Z-CG
Takeoff	60.4 ft	1.32 ft
Before Staging	53.4 ft	1.64 ft
After Staging	62.2 ft	-4.89 ft
Landing (Empty)	53.2 ft	-5.22 ft
Ferry	72.0 ft	-3.17 ft

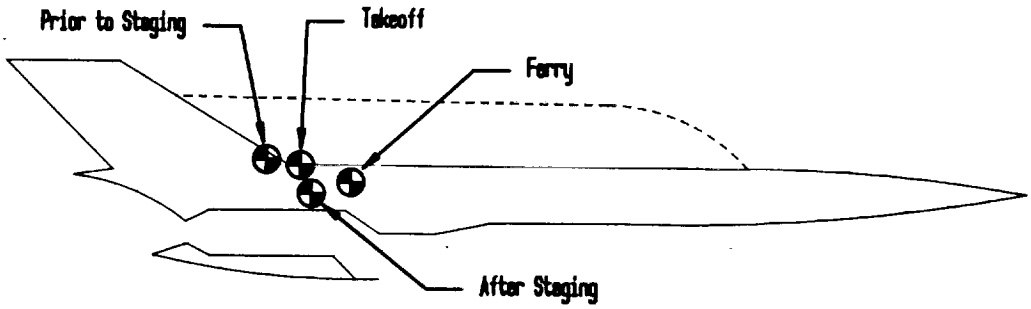

Figure 4.5.4. CG Locations

4.6. Stability and Control

Two flight conditions are necessary for an aircraft to fly a mission successfully. The aircraft must be able to achieve equilibrium flight and it must have the capability to maneuver for a wide range of flight velocities and altitudes (Nelson, Robert. There are two critical phases during the TSTO flight from a stability and control standpoint:

1) Takeoff: Due to its proximity to the ground, the carrier must be able to adjust quickly to sudden changes in its flight regime. Microbursts, thermals, and high winds can induce a sudden change in the direction of the relative wind. This can cause a sudden pitch, roll, yaw, and/or loss of lift.

2) Staging: During staging, great care must be taken to insure that the carrier and orbiter do not collide. Turbulence or the sudden change in its center of gravity could cause the carrier to pitch up into the orbiter.

4.6.1. Static Stability

The more statically stable the carrier is, the less vulnerable it will be to sudden changes in the flight regime. Effective control surfaces will also enable the carrier to adjust quickly to any disturbance and to easily maneuver.

The quickest and easiest way to determine static stability is to find the static margins; if they're negative the system is unstable, if positive the system is stable. First, using a neutral point equation that can be found in several places (in my case, Nicolai), the neutral point was determined by taking into account the lift, drag, and moment coefficients of the wings and canards, aerodynamic center, and angle of attack at five critical points along the flight path. Then, to determine static margins, each neutral point was subtracted by its corresponding XCG location (see Weights & Balances) and divided by the reference chord length. The calculations resulted in the static margins listed in figure 4.6.1.

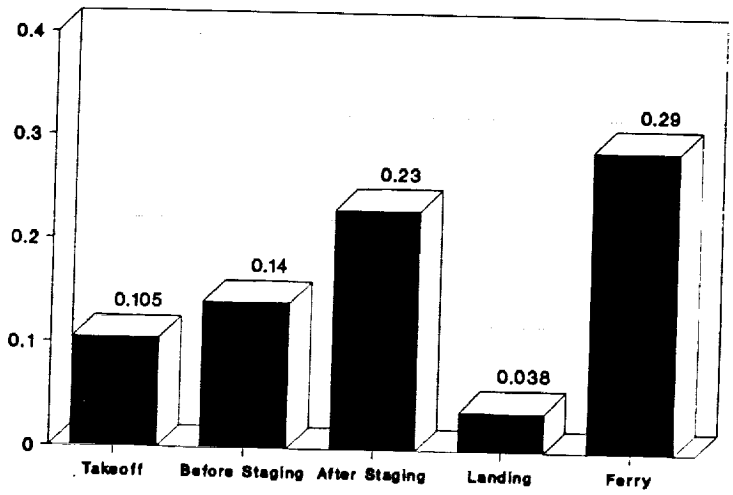

Figure 4.6.1. Static Margins

As one can see, the carrier is stable throughout the flight regime, but perhaps too stable! The highest static margin is over 23% (ferry isn't considered part of the flight regime) making it very difficult to trim. To remedy this, one of three things would have to be done:

1) Enlarge the canard surface area: This would increase drag and introduce heat dissipation problems.

2) Move the wings further forward: This is a viable option, but will considerably alter the carrier's aerodynamics.

3) Move the CG further backward: This can be done rather easily by draining the fuel tanks in a different order, say from front to rear as opposed to rear to front. This is being considered for future design changes.

4.6.2. Control Surface Sizing

The most important control surfaces on the carrier are the canards and the elevons, of which the canards constitute most of the pitching control. Looking at various supersonic aircraft with canards (the XB-70 and the XF-4a in particular) it was found that the wing to canard volume ratio (a simple ratio taking into account both surface areas, the chord length, and the distance between both MACs) hovered between .10 and .11. Taking the lower of the two, the canard surface area for the carrier was calculated at 200 square feet per canard, or 400 square feet total area.

The vertical tail sizes were determined in much the same way. I had at my disposal wing to tail volume ratios of numerous supersonic aircraft (the B-1, F-15, F-16, SR-71, and even the space shuttle) and found, for the twin tailed versions, a ratio anywhere from .12 to .15. Using the average of these two values, the tail surface area was calculated to be 500 square feet per tail, or 1000 square feet total.

Chapter 5. Design Analysis of Orbiter Aerodynamics

5.1. Configuration History

The first Orbiter design configuration was developed by the Aerodynamicist who modeled the shape using a tangent cone (ogive) shape nose with a constant diameter fuselage. The wings were modelled as a delta wing configuration. This design was then modified with a lifting body configuration. The fuselage and the wings were more integrated, as well as the nose. These designs all were developed using the idea that a rocket system would be its main propulsion system.

Later, this configuration was changed so that scramjets could be placed at the rear-top of the Orbiter's fuselage and incorporated as part of the wing. Finally, after analyzing the scramjet system and inlet requirements. The scramjets are still placed to the rear of the Orbiter, but they now are integrated into the fuselage, not the wing. This design makes for a more aerodynamic model and also takes advantage of the volume space that existed and uses that space for the scramjets. See Figure 5.1.

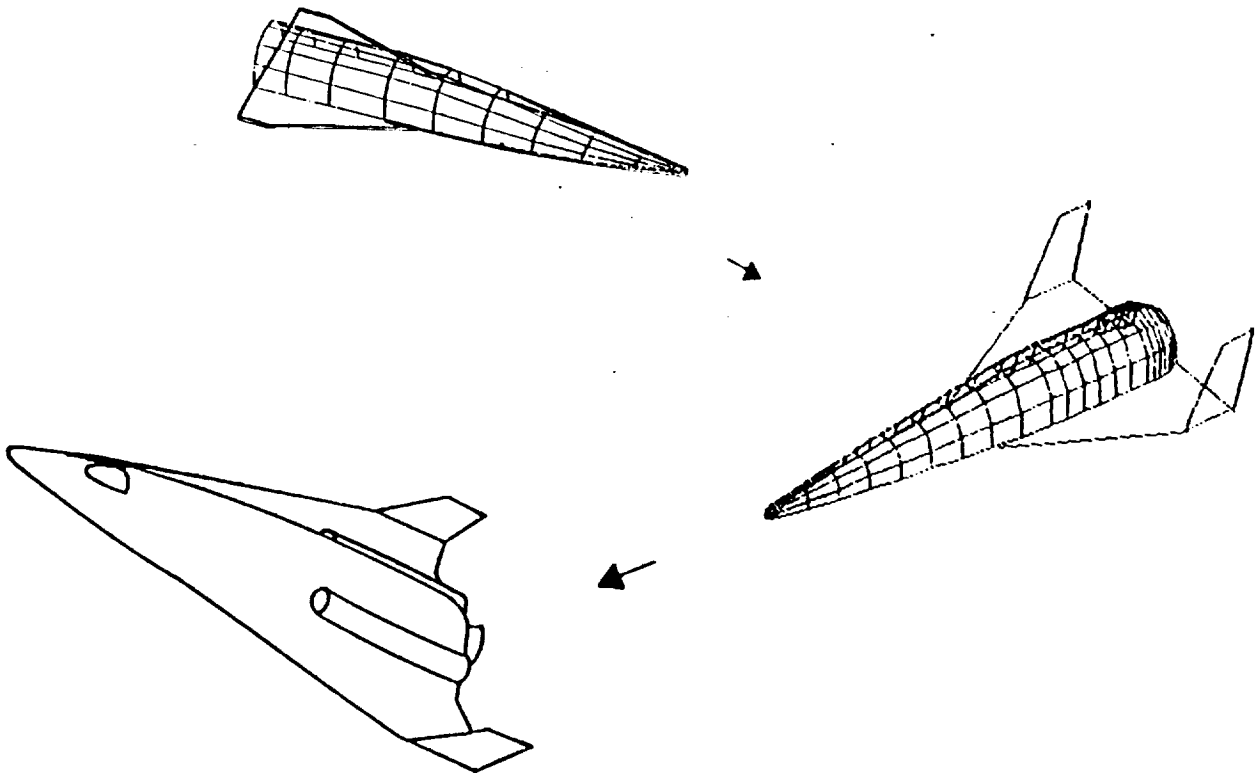

Figure 5.1. Design Configuration History.

5.2 Preliminary Design Concepts

Preliminary design drivers were governed by the trajectory of a hypersonic vehicle through its reentry phase. In this phase, a hypersonic vehicle experiences very low lift-to-drag ratios and as a consequence to this, literally falls out of the sky. It is then necessary to regain steady flight conditions to facilitate the orbiter's glide path to the ground.

It is then generally required that a lift to drag ratio greater than 4 is necessary to pull out of the ballistic type reentry from orbit. For values any less than four, one would be risking a terminally stalled aircraft which would then continue its fall, unable to regain controlled flight and eventually crash into the ground.

Other design parameters included that a cylindrical payload section of length twenty-seven feet and a diameter of ten feet was able to fit inside the vehicle, that high temperatures on the leading edges were to be experienced, and that control surfaces would have to be placed on the vehicle.

Research was done in order to find a hypersonic configuration which produced high lift-to-drag ratios while still fitting the other three design parameters. The chosen preliminary configuration consisted of a half-cone fuselage which obeyed the power law,

$$\frac{r_x}{r_b} = \left(\frac{X}{L}\right)^{\frac{3}{4}}$$

and a delta wing located along the flat side of the cone. This configuration produced a maximum L/D of 5.2 at M=6.8 in test conditions of Reynold's Number = $3.8 * 10^6$ and oriented such that the flat side of the wing-body configuration was parallel to the bottom of the test section. This would then enable the orbiter to be mounted atop its sister aircraft, the carrier. The volume ratio was then defined as,

$$V^{\frac{2}{3}}/S_p$$

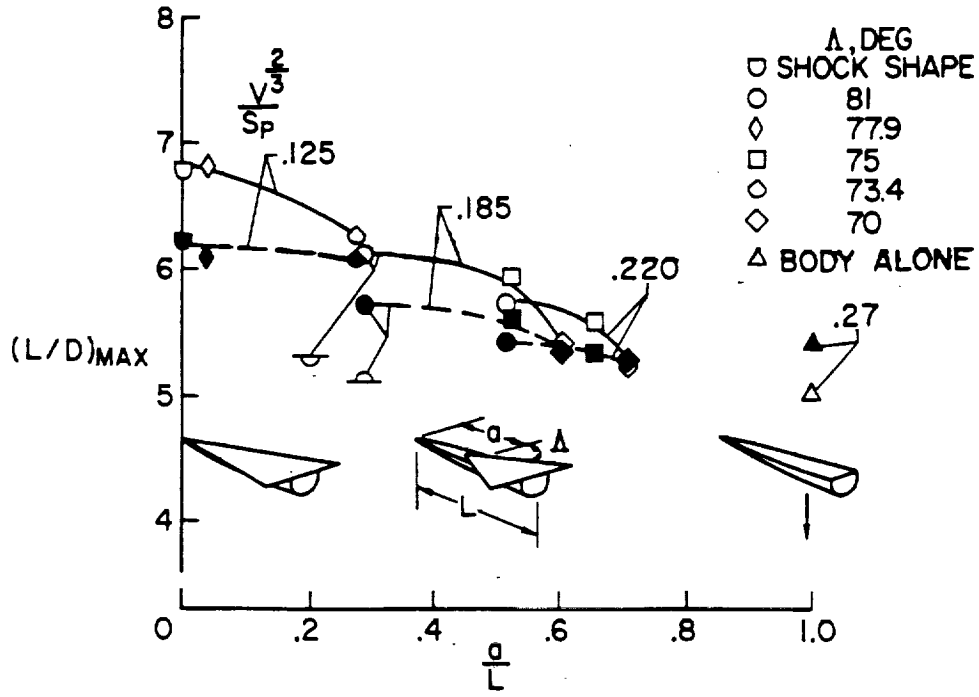

Figure 5.2.1. Characteristic L/D Values for Wing-Body.

where V was the total volume and Sp was the total surface area. Values of both volume ratios 0.185 and 0.220 were considered. It was then noted, from Figure 5.2.1., that for a sweep angle of 70 degrees and a volume parameter of 0.22, the maximum L/D at M=6.8 was equal to 5.2.

It was realized that such a vehicle entering the atmosphere at speeds greater than M=20 would experience extremely high configuration temperatures at its stagnation points. This required that a sharp leading edge was impossible to be maintained throughout the flight envelope. The effect of rounding the leading edge can be observed in Figure 5.2.2. For example, given a leading edge diameter of 3 inches, d, and an overall wing length of 57 feet, L, which implies d/L = 0.004 and L/D max = 5.7 for the shown configuration. Now consider the case that d=4 inches and L=57 feet. Then d/L= 0.006 and L/D max = 5.6 . This showed that the effect of rounding the leading edge lead to optimistic results in the L/D values.

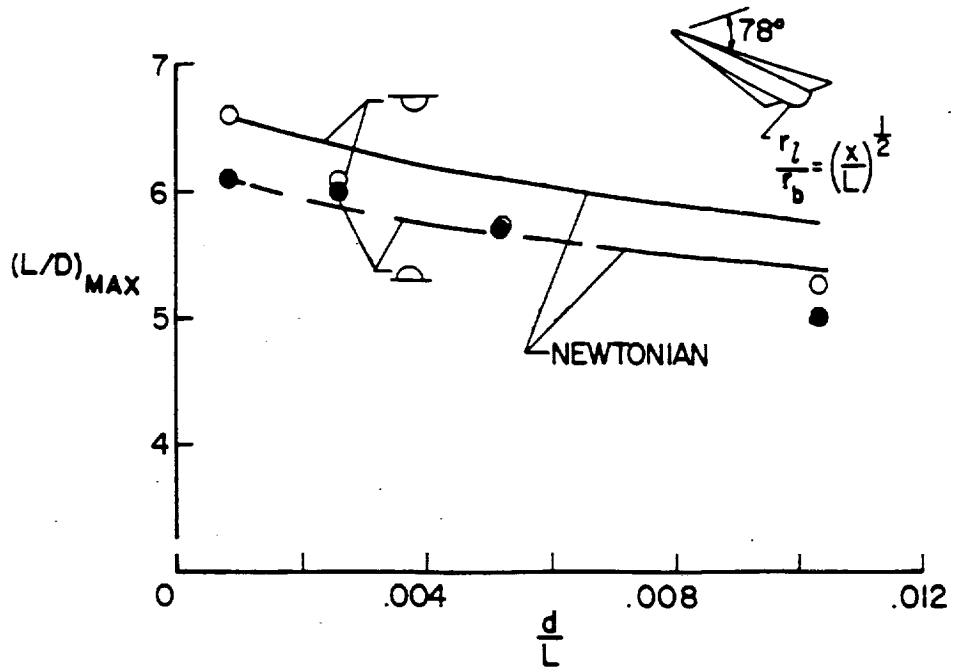

Figure 5.2.2. Effects of Rounding L.E.

Another consideration was to clip the ends of the wings in order that vertical stabilizers could be placed there to maintain stability and control. The effects of this can be seen in Figure 3. Given that the payload was specified to be ten feet in diameter, then placing this into a half cylinder would require that the half cylinder would have to have approximately twice the radius or a diameter of twenty feet.

Then, assuming a typical fineness ratio of 6 between the overall length to the width of the body, then the length of the vehicle was equal to 120 feet. Now consider that vertical stabilizers of base length equal to 25 feet were to be place on the ends of the wing. This gives a c_t/c_r of 0.2 which from Figure 3 does not greatly reduce the L/D characteristics to any noticeable effect.

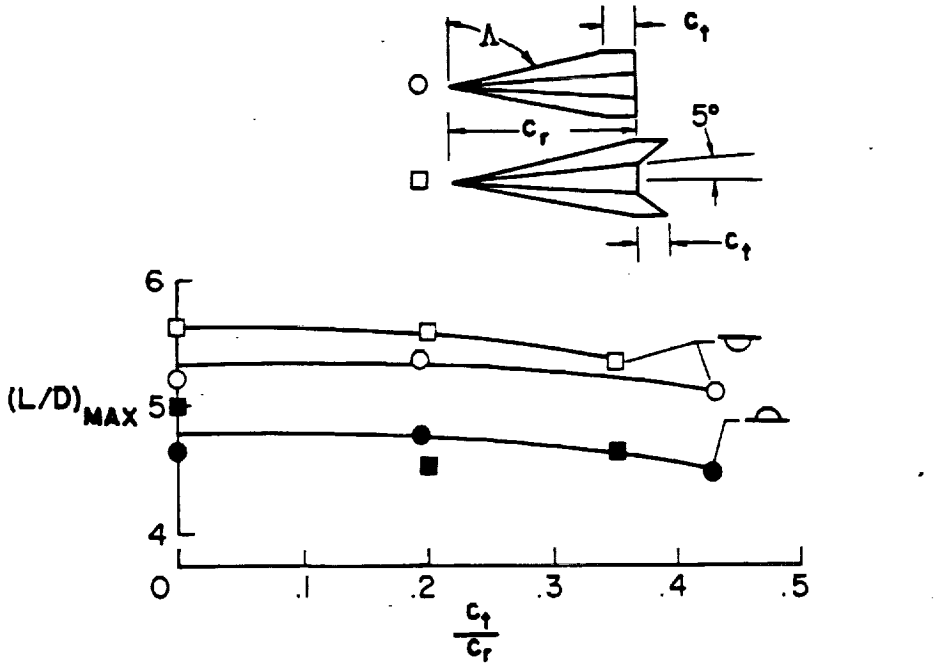

Figure 5.2.3. Effects of Wingtip Clipping.

As a result of the above considerations, the first design iteration resulted in a wing-body configuration of length 120 feet and fuselage width of 20 feet. The sweep angle considered was 70 degrees and the volume ratio was 0.22.

	S (sq.ft)	V (cu.ft)
Nose	1,565	16,611.3
Fuselage	2,215	8,693.9
Wings	2,253	----
Vertical Stab.	490	----
TOTAL	6,523	25,305.2

Table 5.2.1. Surface Areas and Usable Volumes by Component.

Calculations were made to see if the given amount of fuel would actually fit inside the available volume produced by the above configuration. Given a fuel weight of 226,661 lbs and that the engine to be used was a 1/2 SSME (Space Shuttle Main Engine) which uses a liquid hydrogen and oxygen mixture of 1:6, respectively. The density of liquid hydrogen and liquid oxygen was 4.43 and 71.168, respectfully. This then produced a volume requirement of 21,242.4 ft^3. Then the available volume was equal to the total volume minus the volume taken up by the payload, or:

$$V_{avail} = V_{tot} - V_{payload}$$

where,

$$V_{cone} = \frac{1}{2}\int_L \pi r^2 dx = \frac{\pi r_b^2}{2}\int_L [(\frac{x}{L})^{\frac{3}{4}}]^2 dx = L\frac{\pi r_b^2}{5}$$

$$V_{payload} = \pi r_p^2 L_p$$

so, the available volume for the design was equal to (16,611.3 + 10,814.5) - 2,120.6 = 25,305.2 ft^3 . Subtracting the fuel volume + ullage and tank structure (14.285 %) from the available volume, there was 1,028.3 ft^3 left for systems. A summary of the volumes and surfaces of each component is presented in Table 5.2.1.

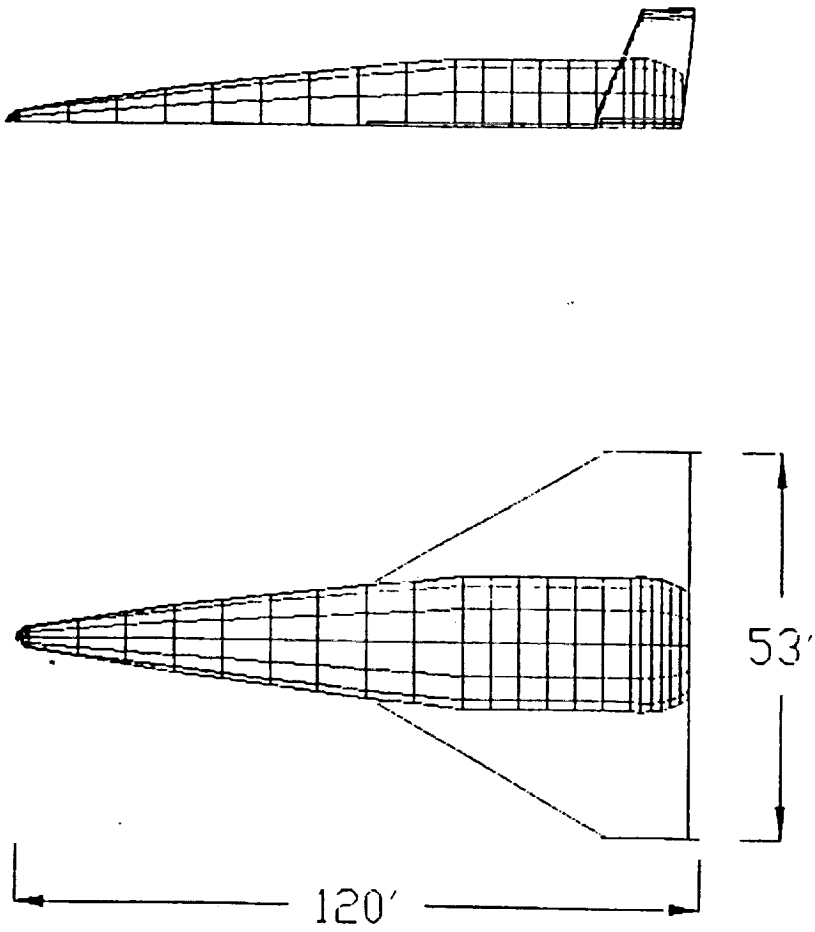

Figure 5.2.4. Preliminary Design Configuration.

5.2.2. Aerodynamic Analysis

The orbiter's design had a length of 120 feet and a wingspan of 53.7 feet at a sweep angle of 70 degrees. Its height was 15 ft. and had a fuselage width of 29.0 ft. The weight of The Orbiter was at 320,000 lbs. These values were estimated for a stage at M=6 at 90,000 feet using one SSME rocket engine. Later, conceptual designs included using SCRAM (Supersonic Combustion Ramjet) engines to reduce the fuel weight.

Rotating the control surfaces outward to increase longitudinal control and increasing the surface area aft of the center of gravity provided increased vortex lift needed to aid landing at low speeds and high angles of attack. Also, strakes placed from the nose to the leading edge of the wing acted as vortex generators to effectively delay separation of the boundary layer and therefore increased the lift at high angles of attack.

The calculations of the lift curve slope, C_l vs alpha, for different Mach numbers followed the method described in Nicolai (reference 1). The subsonic lift curve slope was calculated for an Aspect Ratio of 1.4, which corresponded to a delta wing sweep of 70 degrees, by the equation,

$$C_{l_\alpha} = \frac{2\pi A}{2+\xi^{1/2}}$$

where A = aspect ratio, and

$$\xi = 4+A^2\beta^2\left(1+\frac{\tan^2\lambda_{t/c}}{\beta^2}\right)$$

$$\beta = \sqrt{1-M_\infty^2}$$

The supersonic values for the lift curve slope were calculated from charts taken from reference 5 and are presented in Figure 5.2.5.

Figure 5.2.5 presents some very helpful information. For example, if it was decided that the landing speed of the Orbiter was to be 223 mph or M=0.3, then from Figure 5, CL_{alpha} = 0.026 per degree so an expression for the lift coefficient was obtained: CL = (0.026) * alpha + C1 * alpha^2 . But, CL= W/QS where W= landing weight= 50,000 lbs, Q= dynamic pressure= 133 lb/ft^3, and S=1434 ft^2. Taking C1 (delta wing parameter) of 0.75, CL = 0.26, then solving for alpha, one obtained 9.24 degrees angle of attack to land.

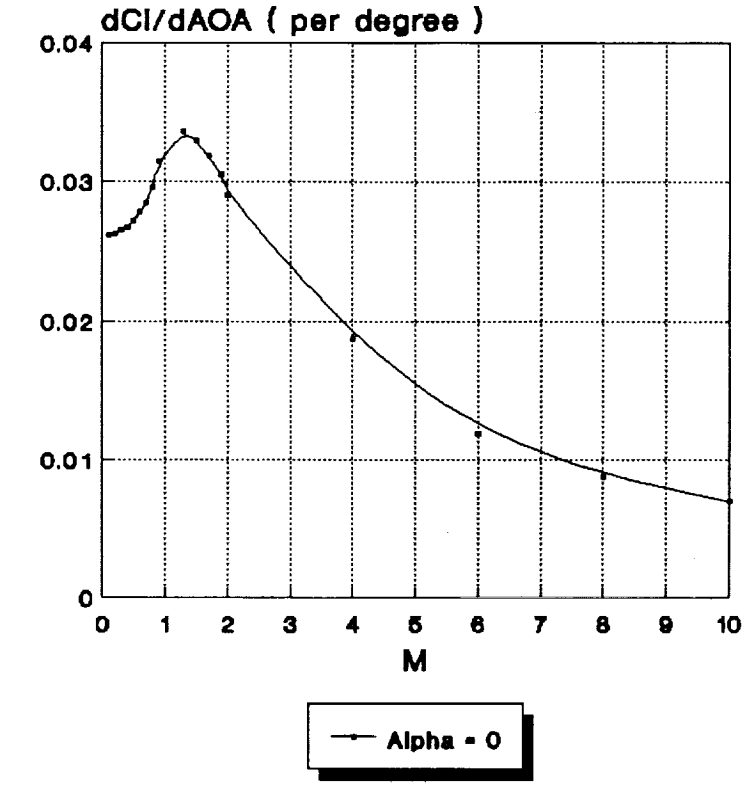

Figure 5.2.5 Lift Curve Slope.

Similar calculations for a landing speed of M=0.2 or 152 mph yielded an angle of attack of 49.7 degrees which was well beyond the stall limit and not recommendable.

An analytical method was used to solve for the coefficients of lift and drag for the design configuration. Given the L/D values for the orbiter (reference 12) the Cl values could be calculated. These values were then used to aid the optimization of the flight trajectory as well as to calculate the stall speeds at given Mach numbers. To find the coefficient of lift, the following equations were used:

$$C_L = \frac{L}{D} C_D \ , \ C_D = C_{D_o} + K C_L^2 \Rightarrow$$

$$C_L = \frac{L}{D}(C_{D_o} + KC_L^2)$$

which is a quadratic in terms of CL. Solving,

$$C_L = \sqrt{[2(\frac{L}{D})K]^{-2} - \frac{C_{D_o}}{K}} + \frac{1}{2(L/D)K}$$

gave values of CL for various Mach numbers.

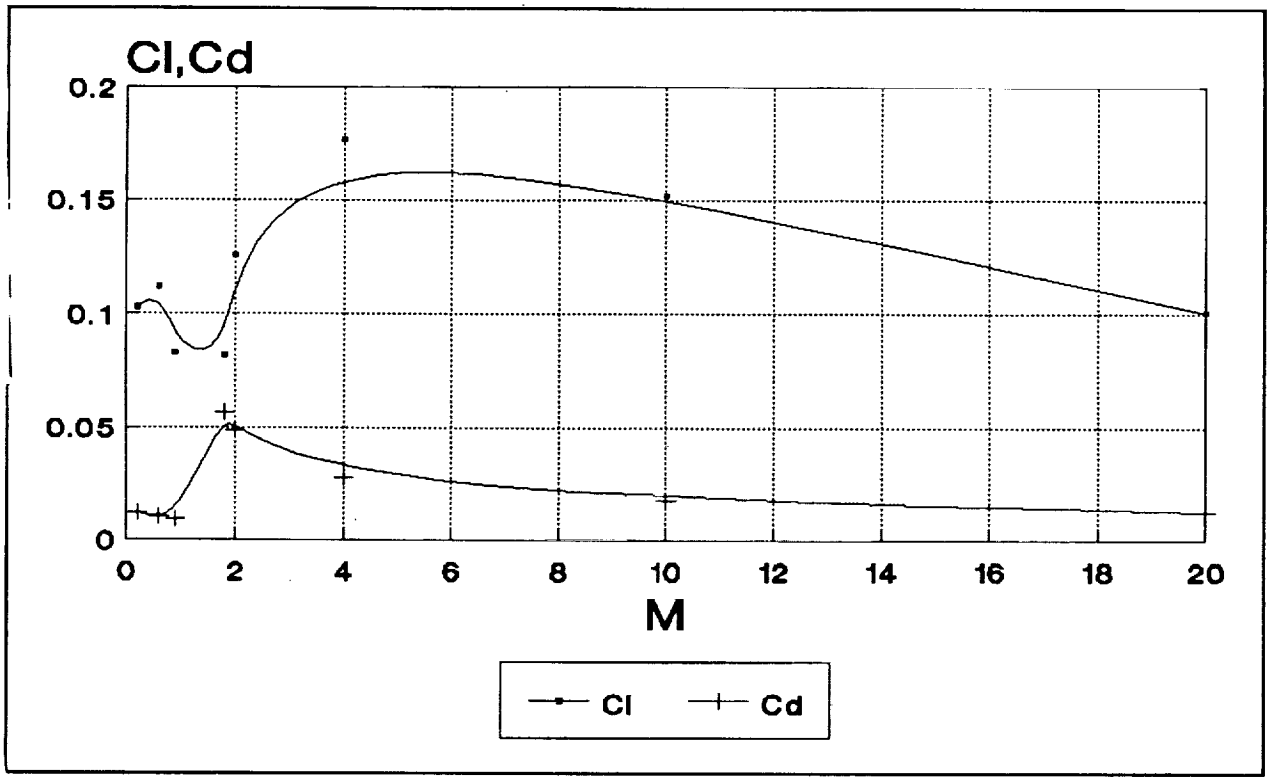

Figure 5.2.6: Cl,Cd versus M.

Analysis of the coefficient of drag was broken into three parts: skin friction, induced drag (drag due to lift), and wave drag. The first two applied to subsonic flow speeds while allthree were considered for M>1. In equation form,

$$C_D = C_{D_o} + C_{D_w} + C_{D_i} \ , \ C_{D_i} = KC_L^2$$

where K = wing efficiency parameter,

$$K = \frac{1}{\pi A e} \quad , \; e = 0.8$$

Each of the terms above were then calculated according to the following components, such as skin friction, induced drag, and wave drag.

The skin friction component was calculated by using the component buildup method in which the orbiter was divided into four parts: fuselage, wing, cone, and control surfaces. Each of these was then associated to a coefficient of friction, CD_f, dependent upon the flow speed and type (laminar or turbulent). The sum of each component times the wetted area ratio, S/S_{ref} was then the total skin friction coefficient and Cd was equal to 1.25 * CD_f, which accounted for interference effects.

The induced drag term was simply equal to the product of the wing parameter, K, and the square of the lift coefficient, CL.

The tangent cone method was invoked to estimate the wave drag due to the conical nose of the orbiter. This analysis involved breaking the cone into linear sections to which a shock cone was associated. Then by summing the contribution of each linear section, the total wave drag component was calculated. This procedure went as follows:

Given that,

$$C_D = \frac{D}{Sq_\infty} = \frac{\Sigma D_i}{Sq_\infty}$$

where Di was the contribution from each section of the cone. Then expanding by noting that,

$$D_i = C_{D_i} q_\infty S = (C_{p_i} + \frac{p_\infty}{q_\infty}) \sin\theta_c$$

the values for the coefficient of wave drag could be readily obtained from tabulated values of Cp for a conical shock,

$$C_{D_w} = \sum \frac{S_i}{S} (C_{p_i} + \frac{P_\infty}{q_\infty}) \sin\theta_{c_i}$$

where S=total cone surface area and $theta_c$=cone angle at each section.

The results found in Figure 5.2.6 show a sharp increase in the drag term as well as a decrease in the coefficient of lift from M=1 to M=2. This illustrated that the drag rise for a delta wing recovered at a higher Mach number than say for example a straight wing which would have come back down closer to M=1.2. In other words, by sweeping the wing, one was able to reduced the magnitude of the maximum drag coefficient but at the same time this cause the drag profile to remain relatively high until a greater Mach number.

By designing a conical nose, the behavior of the produced shock could be anticipated. It was found that at speeds higher than M=6, the shock would indeed hit the tip of the wing. In order to prevent any structural defects due to this, it was specified that the orbiter could not maintain a constant velocity for too long or else the shock would cause structural damage to the ends of the wings. By continually accelerating, the shock would not be located at a stationary point on the wing. Instead, it would sweep across it, minimizing the effect of the shock layer on the wing surfaces.

Later design modifications reduced the total surface area of each of the wing and fuselage components by blending in the fuselage with the wings in order to create additional volume for the housing of Scramjet engines. Also, the radius of the cone for the new design was increase to 15 feet and the overall length was increased to 130 feet. These changes were necessitated by the addition of Scramjet inlets which were included in the new configuration.

The final conceptual design included the addition of strakes from the leading edge of the delta wing to the nose of the cone section, blending the fuselage to the wings and strakes, and rotating the control surfaces 5 degrees from the horizontal way from the fuselage. The final design configuration can be seen with the Scramjet inlets shown.

The analysis of the drag polar followed the procedure in reference 5. The effect of downwash was to deflect the flow from the free stream direction. This resulted in a perturbation in the angle of attack experienced by the flow and the total drag of the orbiter increased. The effect of this inducement from downwash can be observed in the drag polar.

The governing equation for the drag due-to-lift was,

$$C_D = C_{D_{min}} + K' C_L^2 + K''(C_L - C_{L_{min}})^2$$

where K' and K'' were empirically determined from data in reference 5. By selecting a symmetric airfoil, the minimum coefficient of lift was zero for zero AOA. This reduced the above equation to:

$$C_D = C_{D_o} + (K' + K'') C_L^2$$

Note that the minimum drag term from the first equation became the parasite drag term in the second (since the minimum drag at zero AOA is the skin-friction drag for zero AOA). Then, the drag polar could be plotted for various Mach numbers given the minimum drag for those Mach numbers (see Figure 5.2.7). From Figure 5.2.7, it can be observed that as the Mach number increased from M=0.5, the drag polar shifted to the right. This occurred because of the drag rise (see L/D plot) through the transonic region.

Conversely, from M=1.5 to M=6.0, the drag polar shifted to the left. This corresponded to the drag reduction at supersonic speeds. Note that this was due to transition from a normal shock to an oblique shock thereby reducing the component of the flow parallel to the free stream and therefore the wave drag.

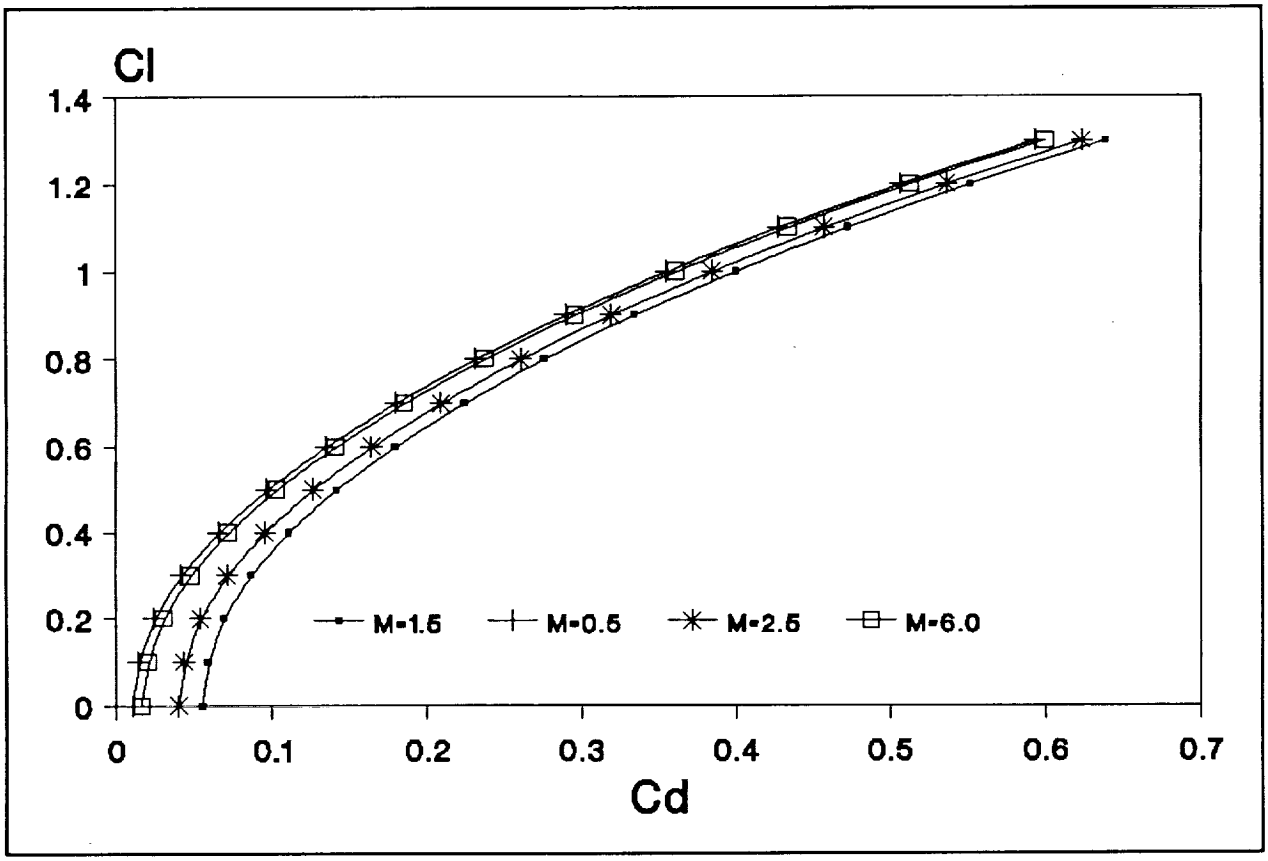

Figure 5.2.7: Drag Polar for Various Mach Numbers.

5.3. Stability and Control

5.3.1. Introduction

Longitudinal analysis was done to ensure the static stability of the aircraft in subsonic and transonic flight. A preliminary analysis using a parabolic airfoil shape showed that such an airfoil would not be as efficient as a symmetric airfoil shape. The effect of camber in the parabolic airfoil was to produce a large pitching moment which at hypersonic speeds would be very hard to counterbalance and therefore not desirable.

Approximate sizing of the vertical stabilizers was done using the method found in reference 1. This resulted in two vertical stabilizers with combined surface areas of 245 ft^2.

The wing pitching moment was calculated using the Air Force's DATCOM manual. This analysis showed the static stability of the orbiter from Mach 0.2 to Mach 1.4, the region of most interest since the dynamic pressure in that range was the lowest and determined the orbiter's landing performance. An alternate method for finding the static margin and the wing-pitching moment slope which followed the procedure in reference 5 was used as a comparison. The data from this procedure ranged through Mach 20 whereas the DATCOM method was only used up to M=1.4.

5.3.3 Longitudinal Static Stability

An analysis using a parabolic airfoil shape was done. Even though the final conclusion dismissed this configuration, the analysis could be useful to discuss.

Given the shape of the airfoil as a mathematical function with respect to the chordwise direction, it was possible to relate the derivative of that function to the pitching moment coefficient about the airfoil's aerodynamic center (reference 7). This procedure involved placement of a vortex sheet along the average chord and integrating each of the vortices contribution to the overall lift.

The analysis showed that for a parabolic airfoil of thickness 5.5", it was possible to land the orbiter at an angle of attack of 9.24 degrees without use of high-lift devices such as elevons. This was a very positive result, however, it was then noted that the airfoil, being cambered, would produce very large pitching moments as the top surface produced a pressure distribution while the bottom was flat and resulted in no pressure gradients. Therefore, it was concluded that another alternative would be more feasible.

5.3.4. Preliminary Sizing of the Vertical Stabilizer

Preliminary sizing of the vertical tail provided an initial estimate to the surface area necessary to maintain control. The necessary equation was,

$$C_{VT} = \frac{l\,S}{bS_w}$$

where l = distance from the wing quarter-chord to the vertical tail C/4 location, S = surface area of the vertical tail (unknown), and C_{VT} was taken from reference 1. The resulting calculation showed that the required surface area was 490 ft^2, or 245 ft^2 per vertical fin. Then, given that the fin was 15 ft long at the root, the height of the fin could be calculated and was found to be 17 ft.

5.3.5. Wing-Pitching Moment Slope

The bulk of the longitudinal stability analysis was taken from the Data Compendium (DATCOM, see reference 7). The procedure for solving the wing pitching moment slope followed 3 steps:

1. Using tables in DATCOM for a wing of given sweep angle, the aerodynamic center parameter Xac/C(r) could be found for various Mach numbers below the transonic range.

2. The transonic values for the a.c. parameter were taken from transonic tables for values up to M=0.8 and from M=1.2 to 1.4. Then a smooth curve was faired between the subsonic and supersonic regions. This resulted in a complete plot of the Xac location versus M (see Figure 5.3.1).

3. From the plot of Xac versus M, the wing-pitching moment could be calculated via the equation,

$$C_{M_\alpha} = \left(n - \frac{Xac}{C_r}\right) \frac{C_r}{\bar{C}}\, C_{L_\alpha}$$

where n= distance from wing apex to the desired moment location in root chords. The values for Clalpha were taken from Figure 5.2.5, and the mean aerodynamic chord was calculated to be 38.2 ft.

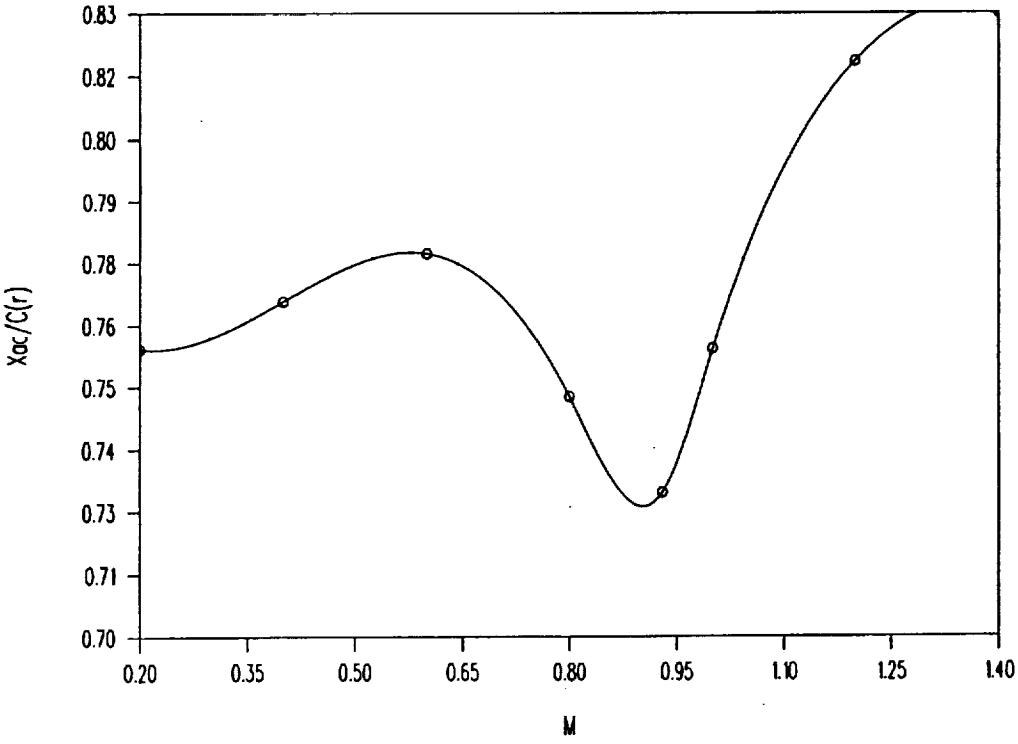

Figure 5.3.1. Aerodynamic Center vs. Mach Number.

An alternate method for solving the wing pitching moment slope was used for the analysis through Mach 20. This involved using the aerodynamic center locations found from DATCOM. With the Xac locations, it was then possible to calculate the static margin by first finding the center of gravity for different load cases.

These cases considered the orbiter with the payload and fuel, with no fuel but with the payload, and with either the payload or the fuel. The equation for the wing-pitching moment slope in terms of the static margin was then,

$$C_{M_\alpha} = -(SM)\, C_{L_\alpha}$$

By calculating the static margin (SM) for each of the considered cases, the plot of the wing-pitching moment slope could be made through Mach 20 (see Figure 5.3.2). The behaviors of the Cm,alpha plot found using either of the methods mentioned above were similar with a slight discrepancy in the transonic range.

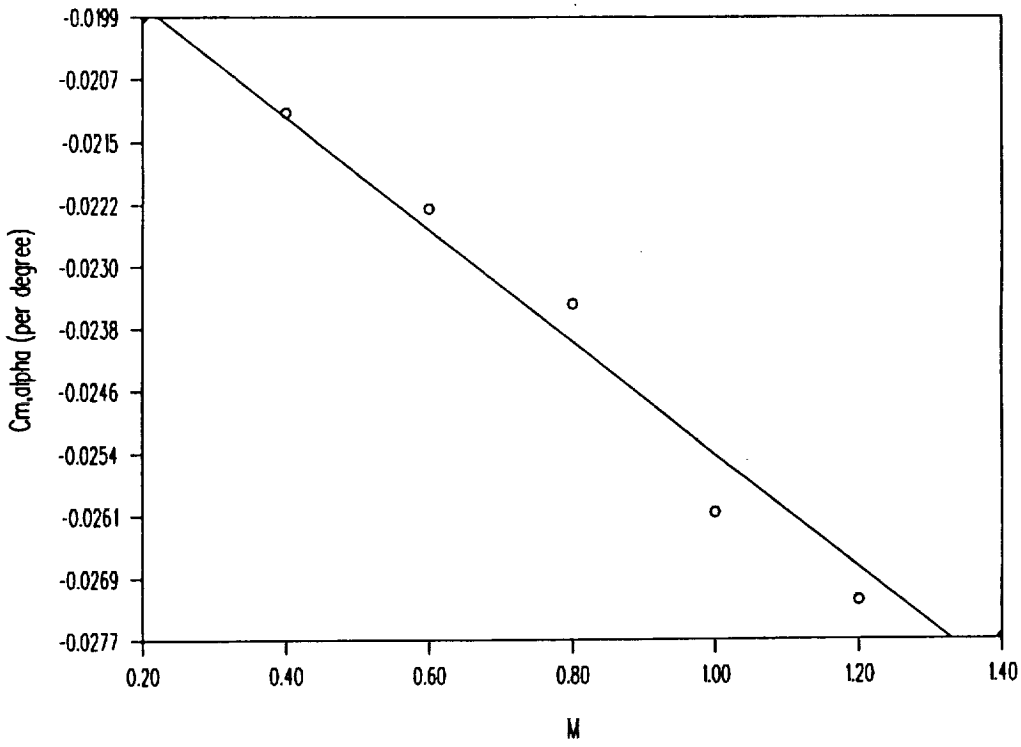

Figure 5.3.2. Wing Pitching Moment.

5.3.6. Pitching Moment Slope for Fuselage

The method for finding the $c_{m\ alpha}$ for the fuselage was obtained from DATCOM. Two methods were presented. The second one was chosen because it was a simpler process to follow, yet still provided accurate results. Its major assumption was that the angles of attack were near zero, which they would be for the orbiter.

The equation used to calculate $C_{m\ alpha}$ was as follows:

$$C_{m_\alpha} = \frac{2(k_2-k_1)}{V_B}\int_x^{x_0}\frac{dS_x}{dx}(x_m-x)\,dx$$

The integral part of the equation was found by stepping through the fuselage. Each one of these steps consisted of 10 feet, until the point of x_0=108.6 ft was reached, which signified the point where the flow ceases to be potential. The rest of the variables represented are as follows:

(k_2-k_1) is the apparent mass factor developed by Munk

V_B is the volume of the body

S_x is the body cross-sectional area at any body station

x_m is the longitudinal distance from the nose to the chosen moment center

x is the location of the center of pressure of a given body segment, measured from the nose

The steps to calculating the integral are found in DATCOM, section 4.2.2.1-3, but are too long and tedious to list here. The final values for $C_{m\ alpha}$ are as follows:

$C_{m\ alpha}$ = 1.655/rad $\qquad$ $C_{m\ alpha}$ = 0.02889/deg

Depending on the units, the appropriate $C_{m\ alpha}$ is chosen.

5.3.7. Center of Gravity

The center of gravity of the orbiter could be found after a definite size and position of alloy components was determined. The calculation of the y-component was quite simple. Since the orbiter was a symmetric aircraft about the centerline axis (which was defined as the y-axis), it was zero. The x-component traveled between the nose and tail. The z-component was between the top and bottom of the orbiter, from a profile view. The following equations were used to locate the x and z components:

$$X_{component} = \frac{\sum(masses\ x\ X_{distance})}{\sum masses}$$

The x-components were measured from the nose. The z components were measured from the bottom of the fuselage.

$$Z_{components} = \frac{\sum (masses \times Z_{distances})}{\sum masses}$$

Results were found for the three possible cases: without fuel and payload; without fuel but with payload; and with fuel and payload. These three cases would be the extreme cases that would be encountered. The final values were as follows:

Condition	X(ft)	Y(ft)	Z(ft)
w/o fuel and payload	86.90	0.0	5.60
w/o fuel, w/ payload	88.50	0.0	5.64
w/ fuel and payload	88.13	0.0	5.90

The center of gravity travels 1.23 ft in the x direction and 0.3 ft in the z direction over the entire trip. The center of gravity is quite small. An often used rule of thumb is that if the center of gravity travel is less than 10% of the mean aerodynamic chord, then it is tolerable. In this case, the 10% value is 3.82 ft. The Orbiter's c.g. location is tolerable.

5.3.8. Static Margin

The static margin is defined as the distance between the neutral point and the center of gravity. It is often used to simplify calculations, such as $C_{m\ alpha}$. In mathematical terms, it is defined as follows:

$$Static\ Margin = \frac{(X_{NP} \times X_{AC})}{\bar{c}}$$

The mean chord of the orbiter is 61.24 ft. The center of gravity had already been found for the orbiter as well. The only term remaining was the neutral point. According to reference 5, the neutral point of a tailless airplane is at the aerodynamic center of the wing-body.

The aerodynamic center was calculated rigorously up to Mach 1.4. Beyond that, the approximation used, according to reference 7, for the neutral point of a tailless aircraft, was 50% of the mean aerodynamic center, of 94.1 ft. The static margin was found using the three different x components of the center of gravity. The following results were produced:

Condition	Static Margin
Fully Unloaded	.188
w/o Fuel and Payload	.147
w/o Fuel, w/ Payload	.156

Notice that the static margin is always positive, which results in a stable aircraft. Although the static margins are a bit high, they all can be trimmed with the use of control surfaces.

5.3.9. Summary

Since the criterion for the longitudinal stability of an aircraft is based on the downward slope of its pitching moment, one noted that the orbiter would maintain a negative pitching slope from supersonic into subsonic speeds down to Mach 0.2 (from figure 2). This result showed that a possible landing at Mach 0.3 was indeed possible from a standpoint of longitudinal stability.

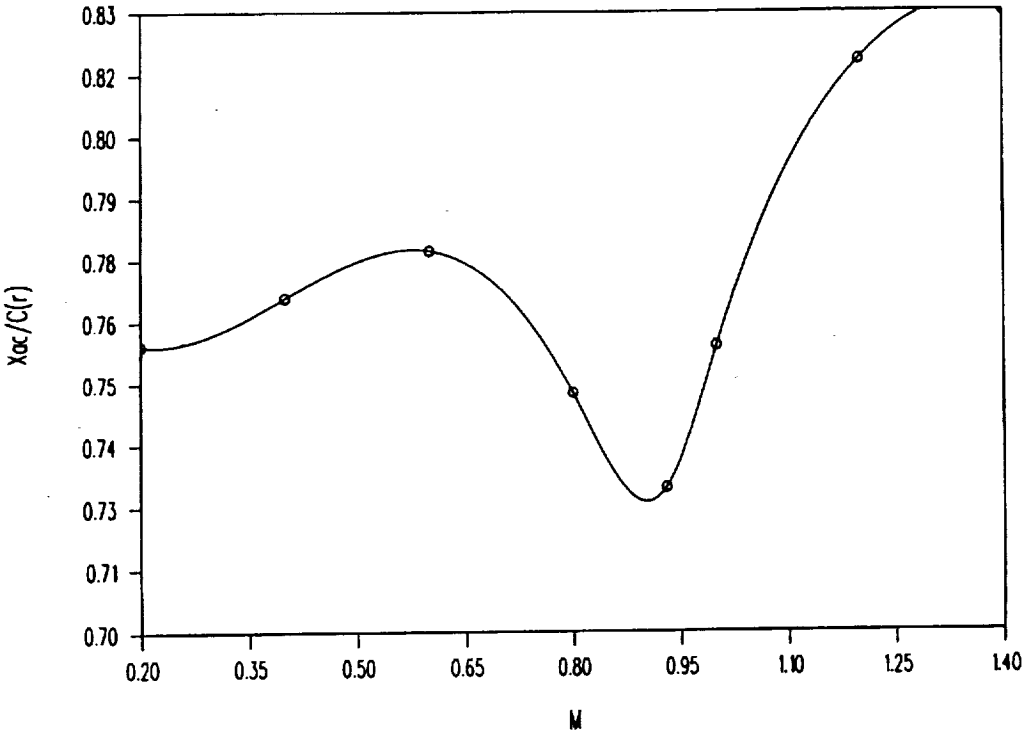

Figure 5.2.3. Location of Xac vs M.

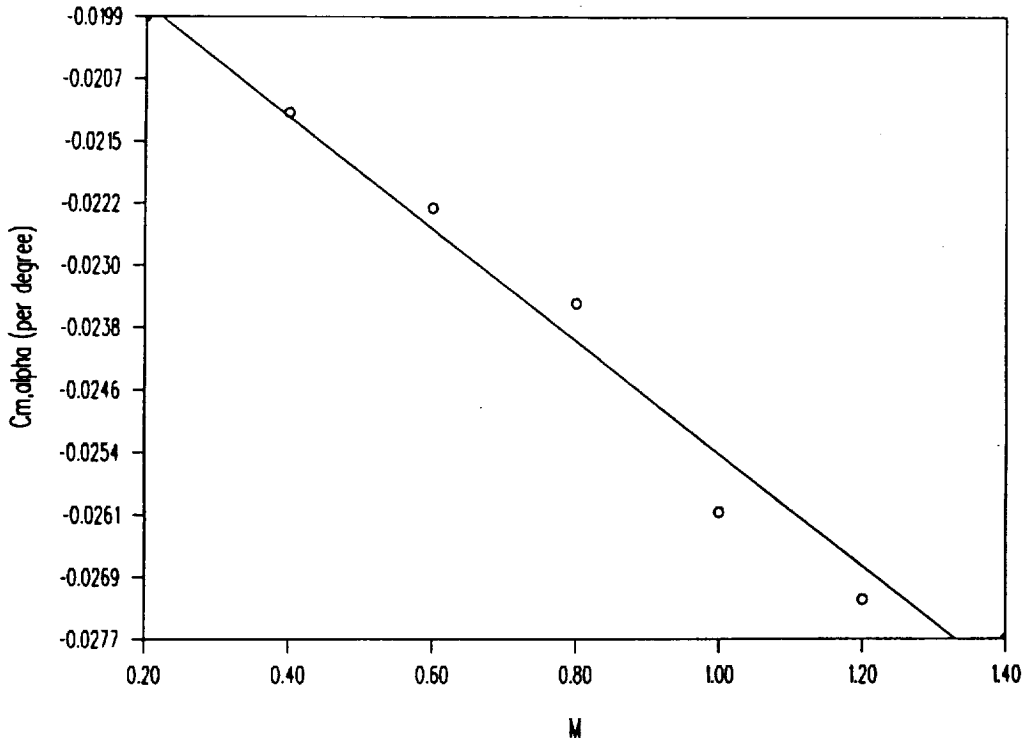

Figure 5.2.4. Wing-Pitching Moment Slope.

5.4. Trajectory Analysis

5.4.1. Introduction

Designing a good trajectory for the orbiter was needed before many design choices could be made. The thermal protection system, orbiter size and overall weight all depended on the trajectory that the orbiter will fly. Due to the important aspect of the design, three different trajectory methods were examined in the early stages of the design process in an attempt to determine the optimum configuration. The methods examined were: an energy method, dynamic simulation, and fixed path trajectory. Each analysis produced very close results which helped validate each method.

The main goal of the trajectory studies was to minimize the fuel used by the orbiter so that the overall system weight could be minimized. The rocket system was examined first due to it's simpler design and ease of modeling. The two types of rocket trajectories examined were a burn-coast method (dynamic simulation) and a full-burn method (fixed path trajectory).

5.4.2. Rocket Analysis

The dynamic simulation involved summing all of the forces on the orbiter: weight, thrust, lift, drag, and centrifugal force. For each time increment of 0.25 seconds, the vehicle's acceleration and resulting velocity changes were calculated. Also, for each time increment the changes in weight due to fuel usage and quantities that were dependant on altitude, such as density and gravity, were taken into account.

The control input for this trajectory program was a data file of angle of attack and throttle setting versus flight time. For intervals of the flight, the orbiter would hold a set angle of attack and throttle setting. The trajectory of the resulting motion was recorded into the data file. Typical rocket trajectories would start at an angle of attack of 6° and end at 0° at the end of the burn phase. These angle of attack changes were to get the needed lift as the orbiter's weight changed while keeping the maximum down range. The burn phase usually lasted 5 to 7 minutes, followed by a coast phase that would last up to 30 minutes.

The first approach taken was to accelerate vertically to escape the denser atmosphere quickly and then start a down range acceleration to orbit. This was to be done by staging at high climb angles (> 45°) and climb to approximately 200,000 ft. The orbiter would then level out it's trajectory and begin

accelerating in the down range direction.

This approach was found to use far too much fuel. The problem was that it was inefficient to lift most of the orbiter's weight using only the rocket engine, which was one Space Shuttle Main Engine. It was next desired to determine which two staging factors, altitude or Mach number, had the most impact on the weight of the orbiter. Analysis produced the following results:

Mach #	Fuel Weight (klbs)
4	250
6	210
8	172
10	150

Table 5.4.1. Effect of Mach # vs. Fuel Wt. for Cons. Alt.

Altitude (kft)	Fuel Weight (klbs)
50	222
60	215
70	208
80	203
90	202

Table 5.4.2. Effect of Altitude on Fuel Weight.

From this fuel weight data, staging Mach number has a greater impact on orbiter weight than staging altitude. It is advantageous to use the denser air to support the orbiter's weight through lift while it accelerates. Also, by accelerating in the down range direction, centrifugal forces will affect the orbiter sooner, which adds an extra component of lift.

The fixed path trajectory method used many of the principles of the dynamic simulation method. Instead of allowing for the changes in the forces to dictate the trajectory, however, a given down range and angle of attack was used as a set parameter. This then allowed for the program to calculate trajectory that followed the set down range distance.

The changes in weights, density, and gravity were considered as well as the forces that acted upon the orbiter. This method produced results similar to that of the dynamic simulation method. Weight values were, however, slightly higher. This method also confirmed one conclusion from the previous analysis,

that fuel weight for a rocket system is dependent upon staging Mach more than upon staging altitude.

5.4.3. Scram/Rocket Analysis

The next method in the trajectory analysis was that of using a combined air-breather/rocket powered propulsion system rather than only a single rocket engine. The air-breathing propulsion system would be used to accelerate the orbiter within the atmosphere to high velocities and the rocket propulsion system would then take over to accelerate the orbiter to the proper orbital altitude and velocity. Due to the hypersonic velocities that the orbiter will be flying at, scramjets were chosen for the air-breathing propulsion system.

Theoretically, the scramjet engines would reduce the amount of fuel required by the orbiter due to the fact that they are more efficient than a rocket engine and they do not require oxidizer to be carried on board the orbiter. Final results will show that a scramjet/rocket powered system can reduce the weight of the orbiter at staging by approximately 63,000 lbs compared to a rocket powered system.

To generate the trajectory of the scramjet/rocket system, the Entry TRajectory ANalysis program (ENTRAN) was selected as the main design tool for the analysis. ENTRAN was given to the Aeronautical design class by engineers from the Flight Dynamics Laboratory at Write-Patterson Air Force Base. ENTRAN is a time stepping analysis package that takes a set of given initial conditions and steps through the trajectory until a final cutoff point is reached.

This package was selected over other methods of analysis because it uses less assumptions than a self made trajectory code and the program was designed with the option to use an air-breathing propulsion system. This allowed the scramjets to be modeled accurately and produce better results.

Work on the scramjet/rocket trajectory began with the establishment of certain operating limits. Two of the most important parameters were the maximum dynamic pressure and the maximum angle of attack. It was important that neither of these values be exceeded so that the structural integrity of the is insured. Values for the maximum angle of attack and other design criteria are listed below:

Maximum angle of attack	4 degrees
Maximum dynamic pressure	1600 lbs
Maximum acceleration	4 g's
Orbital Height	300 miles
Orbital Velocity	25400 ft/s
Low Stage Point Dynamic Pressure	Qstage<1200

For the scramjet/rocket configuration, there are many different variables that need to be examined to determine the most efficient trajectory. Some of these variables are: the number of scramjets, dynamic pressure for a constant Q trajectory, stage altitude, stage velocity, and the point when the scramjet - rocket transition will be made. The first configuration that was examined followed:

6 Scramjets
- Dynamic pressures of 1500 & 1600 lb/ft^2 - Stage weights of 255,000 to 280,000 lbs.

During the scramjet powered phase of flight, it was determined that flying at a constant dynamic pressure would yield the best efficiency. To determine what dynamic pressure to fly at, trajectory's were flown at 1500 and 1600 lb/ft^2. The benefit of flying at the higher dynamic pressure is that more air is going through the engines and the higher airflow yields higher thrust. The benefit of flying at the lower dynamic pressure is that drag is reduced and the chances of encountering problems such as flutter, which occur during high Q flight, are reduced.

Results showed that flying at the higher dynamic pressure was slightly more efficient and saved approximately 1500 lbs. of fuel. Once the higher Q trajectory was chosen, the stage weight of the orbiter was varied to see how adding and reducing the amount of fuel affected the performance of the orbiter. Due to the low thrust of the scramjets, however, this configuration turned out to be under powered and was unable to attain the proper final velocity so no further analysis was possible.

The next orbiter configuration examined employed 8 scramjets for it's air-breathing propulsion system. Using the 1600 lb/ft^2 constant Q trajectory determined from the previous analysis, stage weights for this configuration were varied between 260,000 and 270,000 lbs. After analysis, it was determined that 180,000 lbs. of fuel, which corresponds to a stage weight of 270,000 lbs., would allow the orbiter to attain the proper orbital velocity and altitude. The specification for this orbit can be seen in Table 3 and the trajectory can be seen in Figure 5.4.1.

Stage Weight:	270,000 lbs.
Stage Altitude:	85,000 ft.
Stage Speed:	Mach 6
Propulsion:	8 Scramjets - Mach 6 to 15.5 1/2 SSME Rocket - Mach 15.5 to 28

Table 5.4.3. Initial Trajectory Specifications.

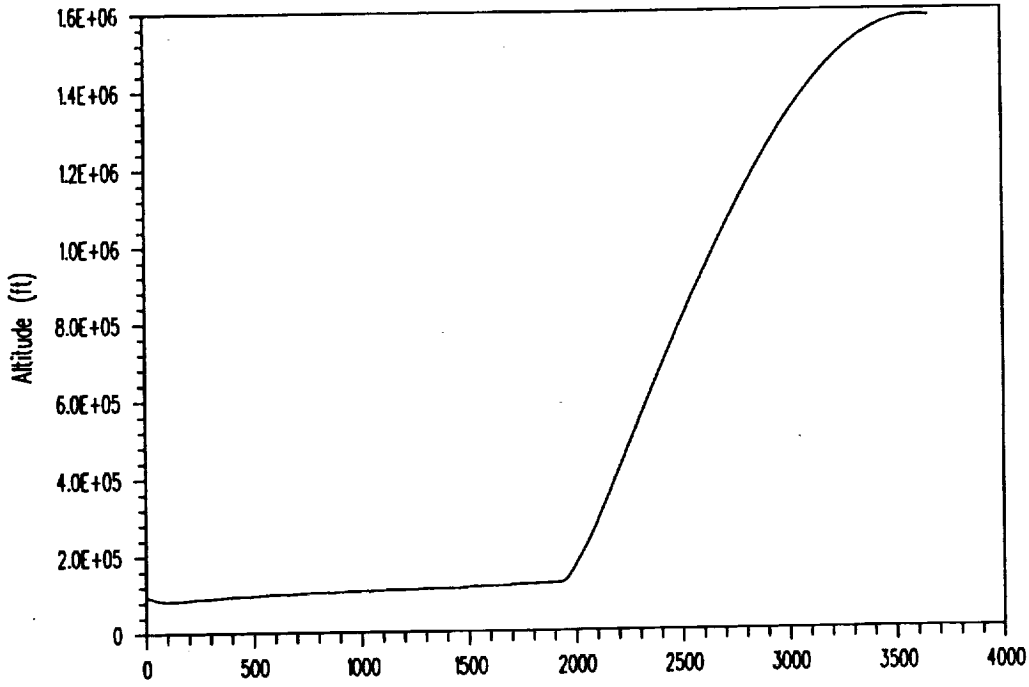

Figure 5.4.1. Altitude vs. Time.

Once a thermal analysis of this trajectory was completed, it was found that the thermal loads experienced by the orbiter were too high and that the weight of a thermal system to cool the skin would drive the dry weight of our orbiter over it's limit.

Taking the information that was gained from the previous analysis, it was combined with input from the thermal and weights & balances analysis and several changes were made to the trajectory. To reduce the magnitude and duration of the thermal loads on the orbiter, the rocket would be turned on earlier in the trajectory at Mach 12. The scramjets were also scaled up 50% (fuel rate and thrust) to help reduce the time spent in the atmosphere.

To determine the optimum staging speed, the graph in Figure 5.4.2 shows the orbiters stage weight for various stage speeds. It can bee seen that for every increase of 0.5 Mach in the stage velocity, the weight of the orbiter drops by approximately 5,000 lbs. Therefore, the higher the stage velocity the lighter the orbiter. The carrier team estimated that they could reach a stage velocity of Mach 6.5 so further analysis keyed on this velocity.

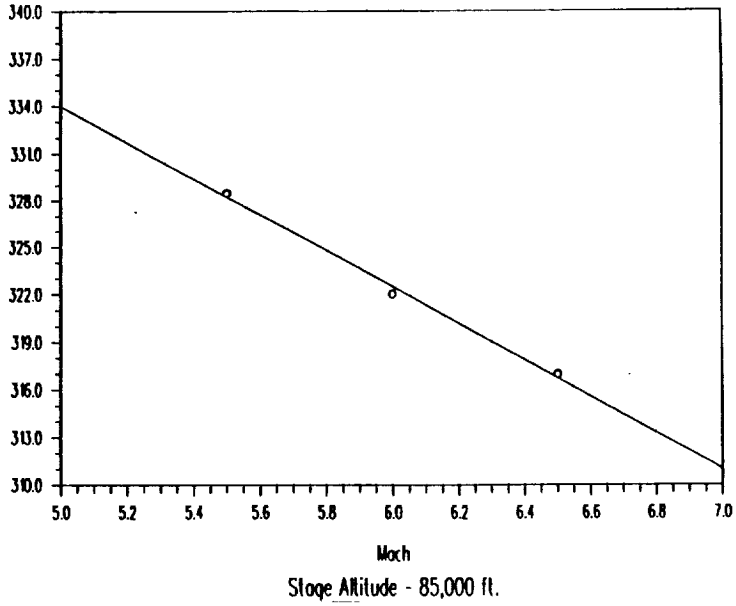

Figure 5.4.2. Stage Weight vs. Stage Mach Number.

Determining the stage altitude was a split effort between the carrier and orbiter teams. After separation, it is planned that the carrier will enter a shallow dive to separate the two aircraft. At such high velocities, even a shallow dive will cause the carrier to lose altitude very quickly. To avoid exceeding their maximum dynamic pressure, the system should separate as high as possible.

The maximum altitude for staging is constrained by the orbiter. A vertical altitude of 90,000 ft is the highest that

the orbiter can fly level at Mach 6.5 and still observe the 4° maximum angle of attack. At higher altitudes the orbiter cannot generate enough lift to fly level. A stage altitude of 90,000 ft was therefore confirmed.

With the stage point defined, a number of trajectories with different stage weights were analyzed to generate the plot in Figure 5.4.3. A stage weight of 317,000 lbs was determined with the orbiter having a dry weight of 90,339 lbs. The results of the final trajectory are listed in Table 5.4.4. Table 5.4.5 gives a mission profile with time and ▲V of the trajectory broken down into it's individual phases. Figure 5.4.4 is a plot of the final trajectory.

For comparison purposes, Figure 5.4.5 shows the trajectory of the scramjet/rocket system next to the trajectory of the rocket only system.

Stage Weight:	317,000 lbs.
Stage Altitude:	90,000 ft.
Stage Speed:	Mach 6.5
Propulsion:	8 Scramjets - Mach 6 to 12 1/2 SSME Rocket - Mach 12 to 28

Table 5.4.4. Final Trajectory Specifications.

Mission Profile	
Scramjet Burn Time	16.1 min
▲V	5436 ft/s
Rocket Burn Time	4.97 min
▲V	13,364 ft/s
Coast Time	35.5 min
Total Time	56.5 min
Total ▲V	18,800 ft/s

Table 5.4.5. Mission Profile.

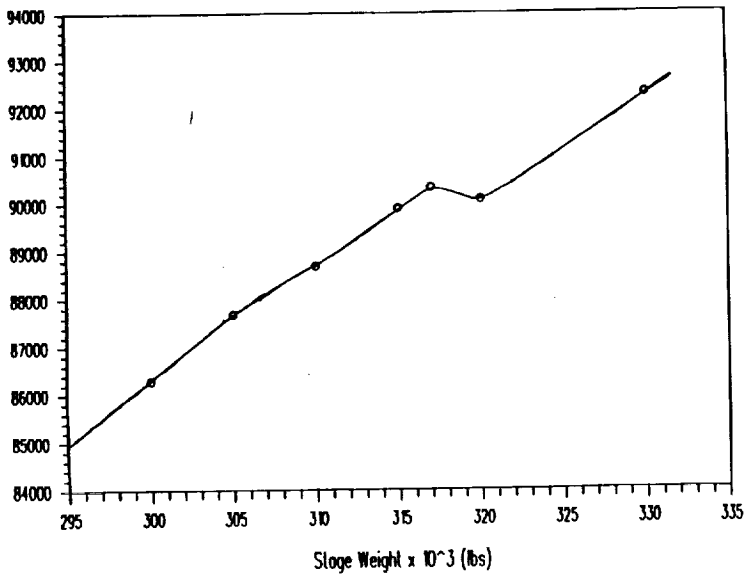

Figure 5.4.3. Max. Dry Weight vs. Stage Weight

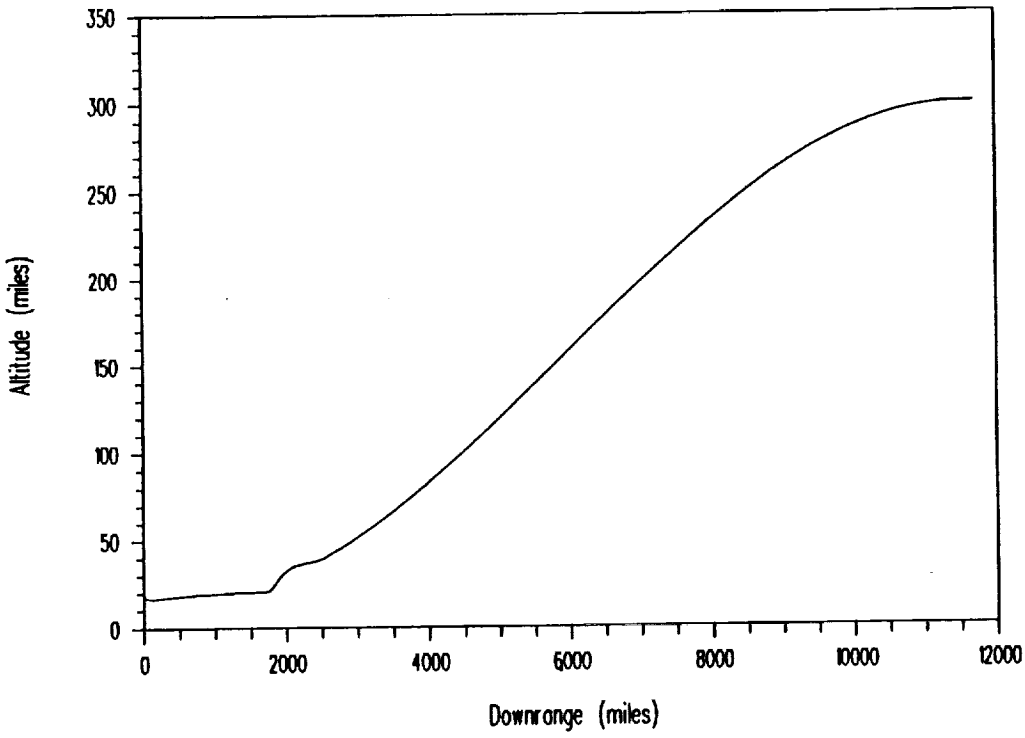

Figure 5.4.4. Final Trajectory- Alt. vs. Downrange

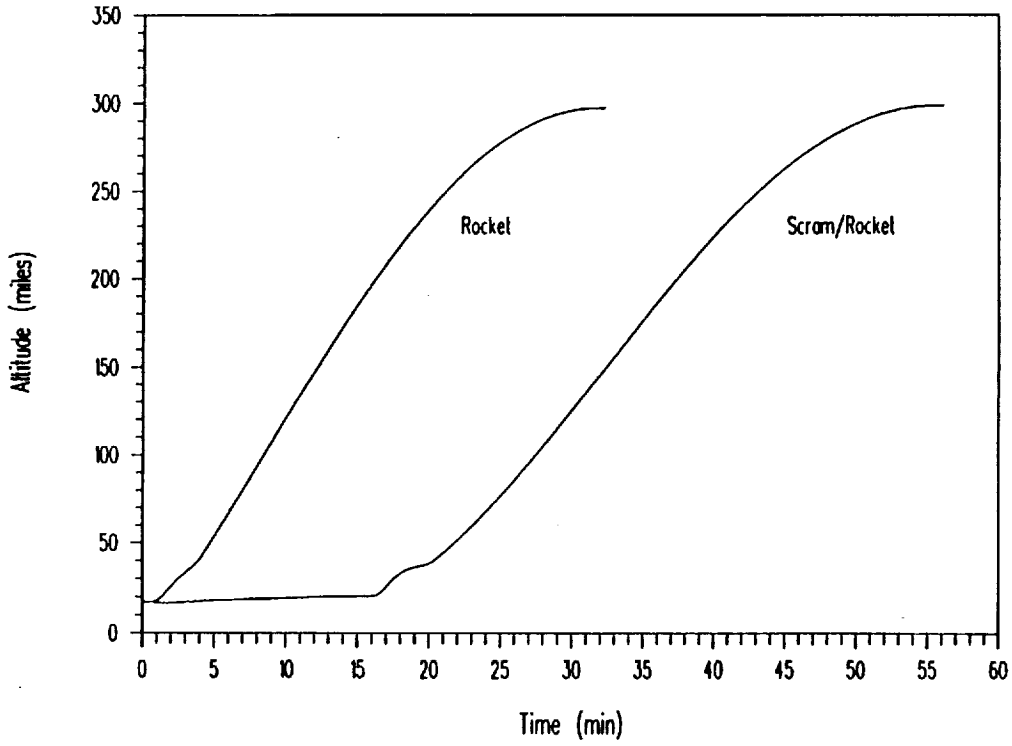

Figure 5.4.5. Comparative Trajectory of Two Sys.

A good example of the efficiency of the scramjets can be seen in Figure 5.4.6. This graph shows the weight of the orbiter over time for both the scramjet/rocket and rocket only configurations. During the powered phase of flight, a steeper slope denotes higher fuel use. Also note the difference in initial weight. The rocket only system weighs 380,000 lbs at stage while the scramjet/rocket system weights 317,000 lbs at stage.

Figure 5.4.7 shows the total acceleration along the X body axis of the orbiter during flight. It is apparent that the scramjets do not expose the orbiter crew to any excessive acceleration. While the crew will experience a 2.7 g acceleration during the rocket powered phase of flight, this is below the set 3.0 g limit and lasts for only 4 minutes.

Most of the trajectory analysis is complete for the ascent phase of flight. The trajectory and thermal management teams are working together to complete the analysis of the reentry trajectory. Should the current orbiter configuration change, the trajectory analysis just described will be executed for the new design. Keeping this in mind, more analysis will be done on the rocket powered and coast phases of the flight to determine if better performance can be gained.

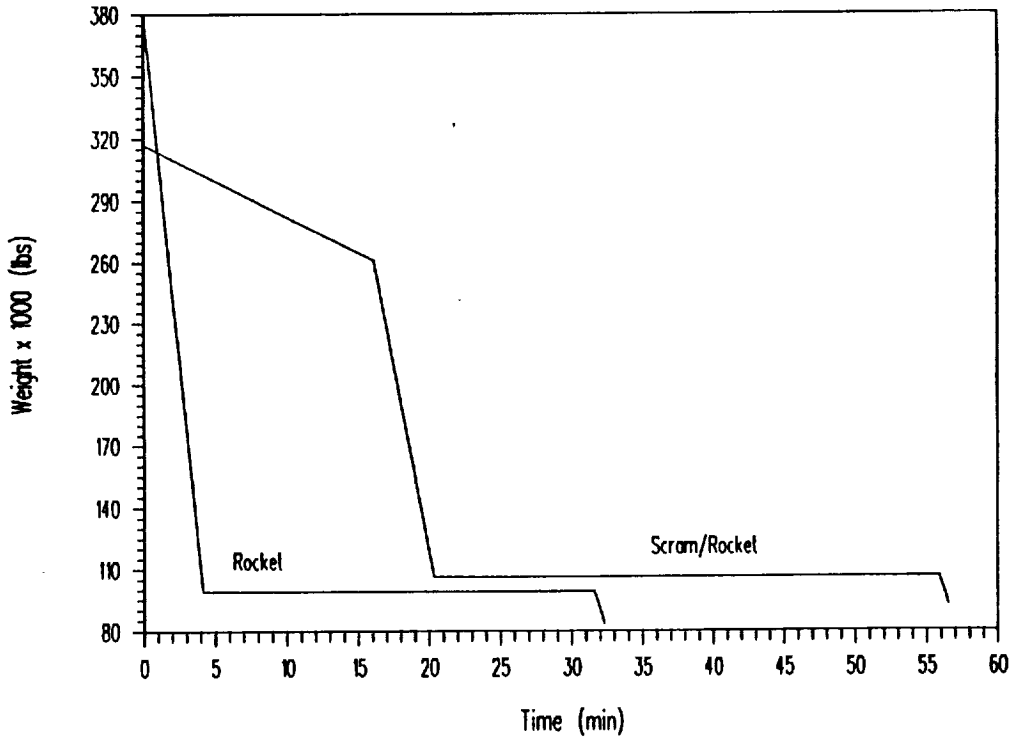

Figure 5.4.6. Efficiency Comparison of Two Systems

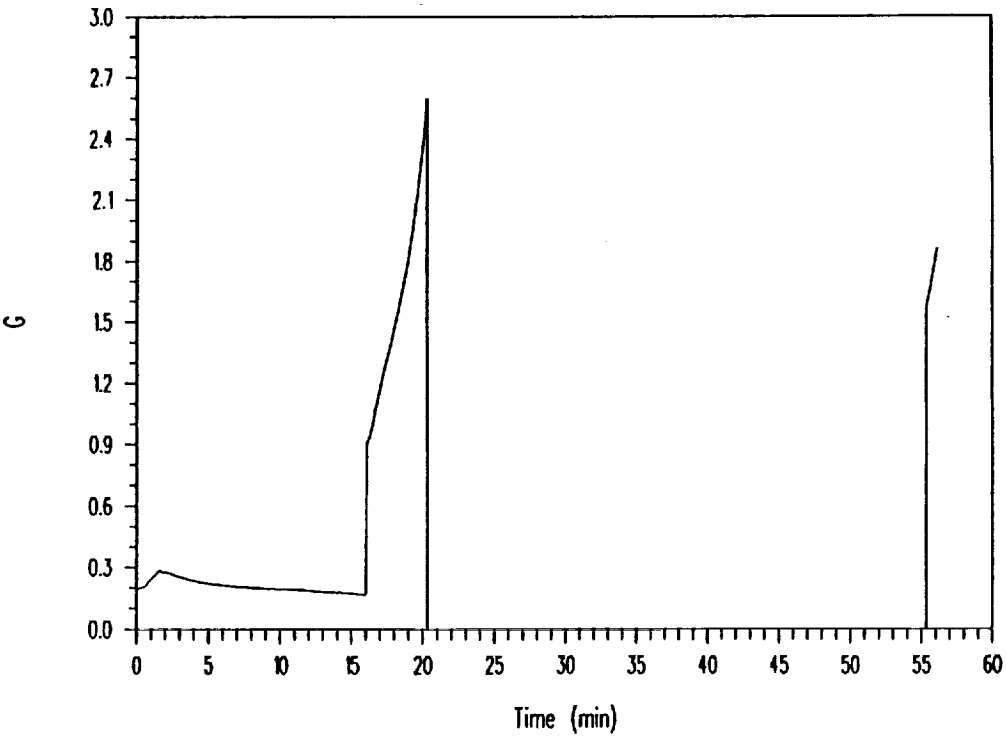

Figure 5.4.7. G-Loading vs. Time

5.5. Propulsion System Analysis

5.5.1. Introduction

A propulsive device, or engine, is designed to generate thrust to overcome the aerodynamic drag on the vehicle with enough remaining net thrust to overcome the vehicle inertia and gain speed and altitude as desired. Generally speaking aerodynamic drag, D, and aerodynamic heating increase with Mach Numbers M^2 and M^3 respectively, for a hypersonic flight at a fixed altitude when the atmospheric density is considered nearly constant. This means that high drag requires expensive propulsive power for maintaining level flights. Also, high heat flux means serious problems for the heat shield to survive the adverse thermal environment and the possibility of having to implement complicated cooling systems.

Drastic changes of the operation environments of hypersonic vehicles call for different engines in different regimes and for different missions. So the selection of engines for a hypersonic vehicle is not dictated by the economics of operation at cruise speeds as it is for conventional airplanes, but by the requirements of significant maneuverability such as orbital transfer or the lift-off from ground into the desired trajectory. The level of net thrust provided by propulsive devices determines the time required to accomplish a mission.

The vehicle altitude is crucial in the choice of the appropriate propulsive devices. Where air is abundant, air breathing engines are preferred since they derive more than 80% of the propulsive medium from ambient air. Where ambient air is not available all the propulsive medium must be provided as propellant carried on board the vehicle, as in rockets.

Obviously, air-breathing engines with a free oxygen supply from the ambient air appear much more attractive than rockets which have to carry the oxidizer along with the fuel. Another important factor is that at high velocities, even the inert nitrogen in the atmosphere can be used to augment thrust because of the larger mass flux of the propulsive medium.

With all this information in mind, two concepts are studied: air-breather/rocket or rocket. The rocket study is done with one space shuttle main engine (SSME) for which there is a vast amount of data and has flown many times. In the air-breather study, an engine that may be used for a greater change in velocity and at higher altitudes is required. Thus, the analysis of a SCRAMjet is done since it is the only air-breather that may be able to perform at Mach Numbers as high as 25 and altitudes up to 200,000 feet.

Then there is the question of fuel. Even though liquid hydrogen has a large volume ratio, it is the only fuel that can maintain stability at high temperatures. More importantly, at around sea level atmospheric pressures, the reaction time of premixed hydrocarbons and air is one thousandth of a second, while that of hydrogen and air is one millionth of a second.

Our choice of engine is the General Dynamics Scramjet, mostly because the manufacturers have provided us with a wide range of experimental data in order to maintain engine integrity while incorporating it in the airframe. In doing so, the only component that has to change is the inlet. The following are the engine dimensions:

* 8 scramjets at 14,174 lbs
* 13.38 ft long
* 3.06 ft wide
* inlet 1.03 ft high at 2067 lbs.
* exit 3.08 ft high

5.5.2. Inlet Design

Inlets are the main source of obtaining air for air-breathing engines. Their purpose is to supply the correct amount of air to the engine. The difficulty in designing the inlets for the orbiter is the wide range of speeds which the craft will pass through while in the atmosphere. At separation, the orbiter will be traveling at Mach 6. It then accelerates all the way up to Mach 12 before the rocket becomes operational. The scramjets are in use from Mach 6 to Mach 12.

The design of an inlet is governed predominantly by the amount of air required of the scramjets to be functional. Before any design can be laid out, this area-of-air-required must be calculated. It is found by first plotting altitude versus Mach number from the trajectory. See Figure 5.4.4.

The altitude versus Mach number graph provides a velocity and density for numerous altitudes. These values are then cross referenced with the graphs of net thrust and specific impulse versus combustor exit fuel/air equivalence ratio for various dynamic pressures. These graphs were provided by the General Electric Company's study of SCRAMjet engines. The graphs are enough to provide values of the amount of air required. According to Nicolai (reference 15, pg. 16-1), the amount of air required for an engine is:

$$A(req) = \frac{m(e)+m(s)}{32.2 \quad V}$$

In this equation, m(e) is the engine airflow in lbm/sec and m(s) is the secondary airflow required for engine cooling, ejector nozzle cooling, etc. For simplistic purposes, it was assumed that m(s)= 0.05m(e). Calculating the area required versus Mach Number provided the following graph:

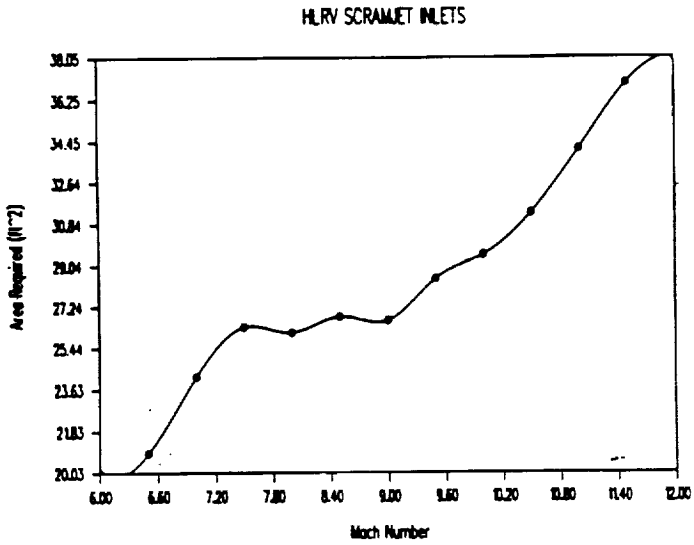

Figure 5.5.1. Area Required Graph.

It must be noted that the area required is based upon the altitude. Thus, this particular graph is only good for the trajectory in Figure 5.4.4. If another trajectory is used, another graph must be created.

As obviously seen from the graph, a wide range of areas will be required for the engine. The area required continuously increases as Mach number and altitude increase. Such an effect is due to the drop in density as altitude increases and the needed increase in thrust.

The primary difference between SCRAMjets and all other types of engines is that combustion will take place supersonically. Thus, flow does not need to be subsonic like those of subsonic-

combustion engines (ramjets, turbofan-ramjets, etc...). However, airflow used in the combustion process should not be hypersonic.

One of the first considerations in designing an inlet is to determine whether a variable or fixed inlet will be used. The advantages of having a variable inlet are the capability of maintaining the compression shock at the lip of the cowl which produces the best efficiency for the engine. On the other hand this will increase the aircraft weight do to the hydraulic mechanisms required. Then we look at a fixed inlet which doesn't have the burden of extra weight but is less efficient. A document from NASA Langley (NASA-TM-X-2895), "Design Considerations for the Airframe Integrated Scramjet," and other studies deduce that the fixed case is preferred. This all stems from the fact that scramjets are used at high mach numbers and the combustion is at supersonic speeds.

With such an attractive performance potential, when designed to have full air capture at or just under the cruise mach number, it can produce high pressure recovery over a wide range of mach numbers with high air capture at low angle of attack. Our trajectory shows a climb at low angle of attack and a linear mach vs. time. To determine the pressure rise in the shock train that precedes the combustion, it was important to accomplish this by using simplified frictionless flow with constant specific heats.

Some guidelines for this propulsive cycle are: cowl lip and wave drag must be low, at the end of boost the air capture ratio should be no less than 0.6 to 0.7 of the maximum air capture ratio, the inlet contraction ratio should be enough to provide combustion to free stream mach ratios of 0.3 to 0.5.

In order to avoid reentry problems with the engines and have the capability of ignition prior to staging, it was decided to place the engines on top. Four scramjet modules are placed in the arc of the body cylinder starting at the wing. To avoid interference with the nose shock, the engines only stick out one foot above the cylinder radius. The inlet ramp is then angled down at 10 degrees with a 2 ft. drop and a length of 28.92 ft. Great difficulty is encountered in the inlet design of this orbiter because of its controversial composition. The free stream flow first encounters the shock at the nose, it is compressed until it meets an expansion of 12.6 degrees where it is channeled to the 10 degree ramp compression, and finally it is lead to the inlet. The entire process is analyzed as a cone. Since the ramp begins only 19.26 ft from the leading edge, this brings up the question of how the airframe interference will affect the flow. Unfortunately, the answer to this falls under an analysis that is beyond the time, knowledge, and experience of this course.

5.6. THERMAL SYSTEMS

5.6.1. Introduction

Heat transfer is a significant driving factor in the design of hypersonic vehicles. The design of a hypersonic vehicle is dependent upon the geometry of the nose cap and of the leading edges of the wings and fins. For example, when a vehicle is accelerating in the atmosphere a very sharp leading edge will produce higher stagnation temperatures than will a very blunt leading edge. This occurs because the blunt edge creates a stronger shock and therefore disperses more heat into the atmosphere rather than onto the vehicle. The drawback of the blunt edge is that it also causes greater wave drag.

Aside from the vehicle's geometry, the heat transfer also depends on the velocity, the altitude, and the structural materials and the time of exposure. As the velocity increases, the temperatures will also increase. However, as the altitude increases the temperatures will decrease. This results from the fact that the air becomes less and less dense the higher one goes.

The time of exposure is important in that, should the vehicle be subjected to extremely high temperatures for only a short time(say less than 6 minutes), the structure would not "feel" these temperatures due to the heat transfer time delay. So, one could design for the lower temperatures at which the vehicle would be cruising. However, it should be noted that it would be unwise to use this design technique and then try to cruise at these higher temperature ranges.

5.6.2.Method of Analysis

The method of heat transfer analysis chosen comes from a computer code called CDHEAT which stands for Conceptual Design Aerodynamic Heating Analysis. Unfortunately, proper credit cannot be given for the origin of this code is somewhat of a mystery. The code itself is based on curve fits on extremely detailed analyses of specific geometric shapes. These designs that were analyzed using CDHEAT are: 1) hemispherical nose cap, 2) cylindrical wings or fin leading edges, 3) delta wings, 4) cones, and 5) fins.

The general approach of CDHEAT comes from establishing heat transfer coefficients. The geometry effects are accounted for by normalizing the coefficients with an appropriate reference value. The code supplies separate reference values for laminar and turbulent flows and is applicable to windward and leeward surfaces. Each reference value is dependent upon only free

stream speed and free stream conditions.

The procedure taken involves first modelling the given vehicle into the simple geometric shapes. Certain shapes like the cylinder have corrections for a forebody. Next, the reference heat transfer coefficients are calculated. These are functions of the Mach Number and altitude. Then, the ratios of the heat transfer coefficients are calculated. These depend upon which geometric shape is being considered, the free stream conditions, the angle of attack, the Mach Number, and whether laminar or turbulent flow is being considered. Finally, the heat transfer rates and wall temperatures are calculated by an iterative process from:

$$q = o\ E\ Tw^4 = href\ h/href\ (Taw - Tw)$$

where:

E = Emissivity of the skin material
o = Stephan-Boltzmann's Constant
q = Heat transfer rate (BTU/ft^2/sec)
Tw = Wall Temperature (F)
Taw = Adiabatic Wall Temperature(R)
href = Reference heat transfer coefficient
h/href= Heat transfer coefficient ratio

5.6.3. Design Procedure

There were two main design goals set at the beginning of the project. One was to design a Thermal Protection System (TPS) that would allow the orbiter to safely transverse all phases of the mission. The second was to minimize the weight of the TPS in order to enhance the orbiter's performance. These are typical design goals for any hypersonic vehicle where weight efficiency is desired. However, due to the nature of the orbiter's ascent trajectory (which is due to the use of SCRAMjets), these goals are even more demanding since the orbiter would "feel" the high temperatures because of the long exposure time.

With the CDHEAT code set up to accept an inputed trajectory the temperatures could now be calculated. The stagnation temperatures along all of the leading edges were the first concern. The nose cap radius was set to 6 inches and all other leading edge radii were set to 3 in. Also, the wing sweep angle was set to 70 deg. and the fin sweep angle was set to 30 deg. The maximum temperatures on the nose cap and the wing leading edge were within the boundaries of conventional TPSs. However, the maximum temperatures for the fin leading edges were at about 7,000°F. This was extremely high.

Therefore with the consent of the stability and control team

the sweep angle was increased to 55 deg. Now the fin also was within reasonable limits of thermal protection. A graph of Temperature vs. Time is illustrated in Figure 5.6.1, while Figure 5.6.2 displays their Heating Rates vs. Time.

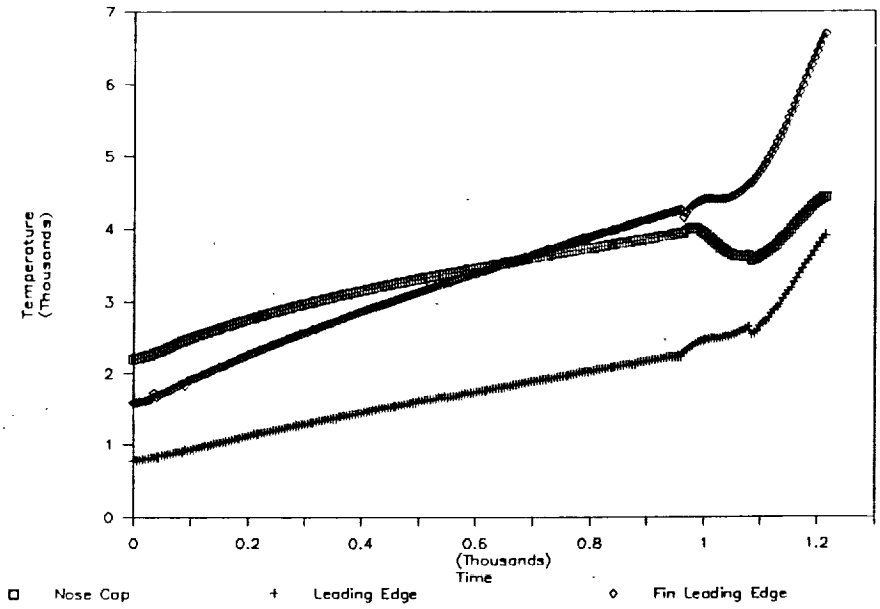

Figure 5.6.1. Temperature vs. Time.

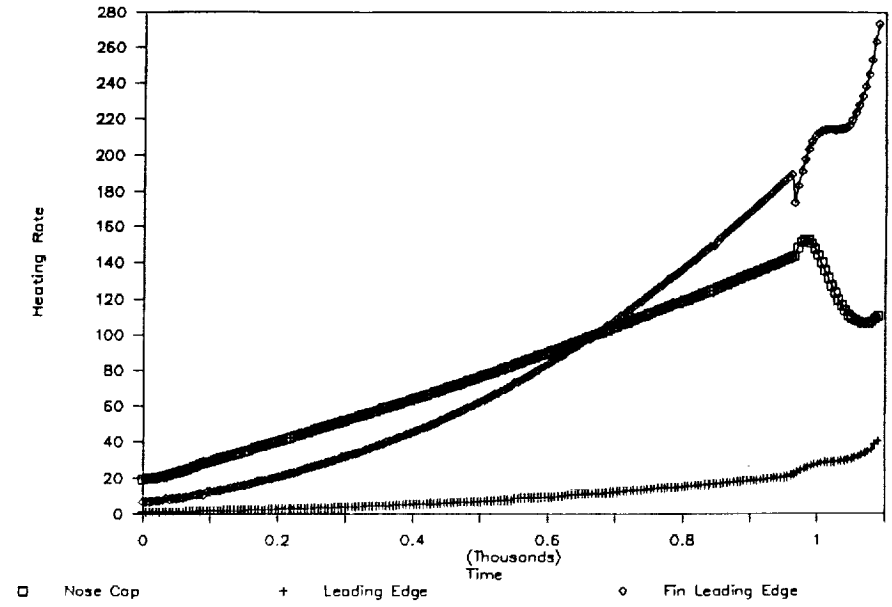

Figure 5.6.2. Heating Rates vs. Time.

Looking over the graph one notices how the curves are very smooth until at one point there is a kink and they all shoot up. This kink is where the rocket is turned on. From this point on it is not much longer before the orbiter is out of the atmosphere altogether.

With this information in hand a suitable TPS was researched for the orbiter. Unfortunately, at this point in time, no materials can provide structural support under these thermal loads. The few materials (such as carbon-carbon composites) that can withstand these temperatures without an active cooling system need to be replaced every other trip. So a passive TPS (i.e. heat shielding) was ruled out for these parts. After all one of the requirements of the project is that the orbiter be reuseable. Therefore active cooling systems were then researched.

The following active cooling TPS information comes mainly from NASA Contractor Report-1916. Spray cooling was determined to be the most efficient means of dealing with higher heat fluxes and temperature levels. This is exactly the case at the nose cap and is the reason for using spray cooling at the nose cap. The choice of coolant was to be determined next.

The two coolants investigated were Lithium and Water. Rather surprisingly the water was found to have the lower system weight and was the coolant of choice. A diagram of the typical water cooling apparatus is displayed in Figure 5.6.3. The procedure for a weight estimation of the system is given on p. 156 of CR-1916. The orbiter's spray system was estimated at 141.3 lbs.

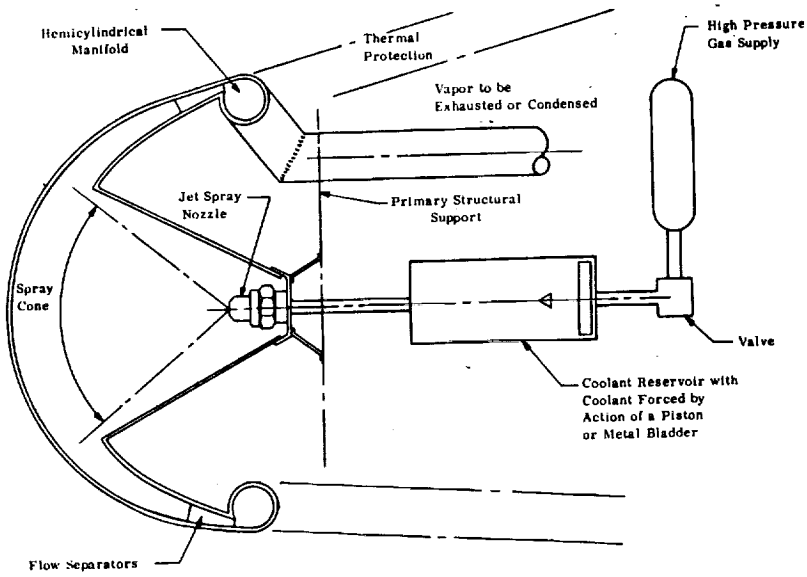

Figure 5.6.3. Typical design of Spray Cooled L.E.

The report had also concluded that for a wing leading edge

the most efficient means of active cooling was either transpiration cooling or indirect convective cooling. It states that transpiration exhibits superior heat transfer and blocking characteristics, but weight penalties due to expended coolant , porous material and the plenum chambers overshadow its thermal advantages. As a matter of fact due to the low coolant flow rates the aerodynamic advantages usually associated with wing drag reduction are of an insignificant margin.

With this information in hand plus the fact that the porous materials are susceptible to clogging, the indirect cooling method was chosen for leading edges of the wings and fins. Again a coolant was needed for the system. This time the two investigated were water glycol and silicone. Using the weight analysis methods on p. 129 for liquid convective cooling, the two were compared head to head with variations in the sink temperatures of each. The winner was silicone which has the following characteristics:

$Cp = .43$ BTU/lb/°F
$Ts = 300$°F
$To = 400$°F

The weight of the wing's system was 529.9 lbs. The weight of the fin's system was 2370. lbs. A schematic of the apparatus is displayed in Figure 5.6.4.

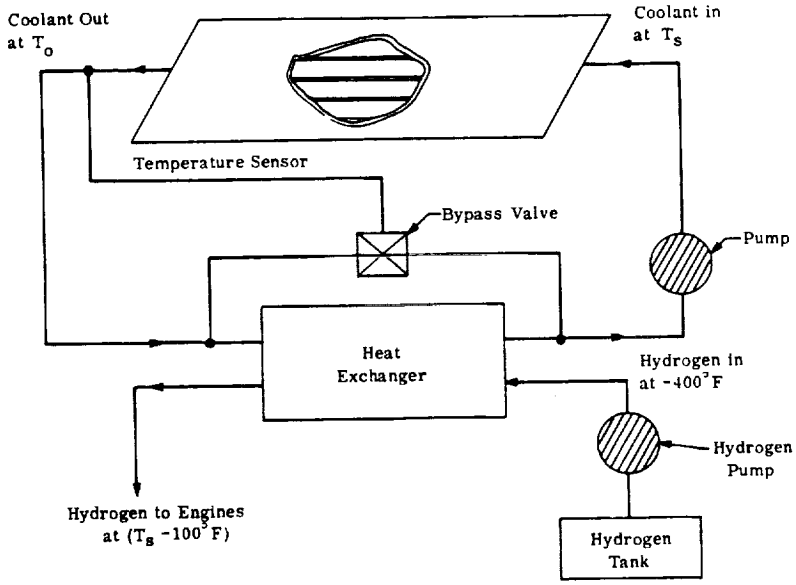

Figure 5.6.4: Indirect Liquid Convective Cooling Schematic.

Now the belly of the orbiter had to be protected from the intense heat of reentry. Carbon-carbon (c/c) composites were placed here. They are good for multiple cycles when a silicon carbide coating is applied and the maximum temperature experienced is only around 2200°F. The weight of the shield was estimated to be 1.1 lb/ft^2 over the area covered.

The weight of the entire TPS is summed up in Table 5.6.1 and was found to be 9502.4 lbs. Due to the uncertainty of the weight estimation method, there was a margin of excess weight allocated for the thermal protection system. Also, the TPS components are listed in Table 5.6.2.

TPS	Weight (lb)
Heat Shield System Spray System Indirect Convection	6461.2 141.3 2899.9
Total System	9502.4

Table 5.6.1. Thermal Protection System Weight Analysis

Thermal System	Components
Passive	Heat Shields
Active	Spray (Nose) Indirect Convection (L.E.)

Table 5.6.2. TPS Components

5.6.4. Materials

In researching a structural materials that would allow for the lowest weight and highest operating temperature, it was narrowed down to nickel-based superalloys and titanium alloys. Almost all nickel-based alloys retain their strength up to about 1400°F. However, there is some question as to their temperature oxidation resistance. On the other hand there are two titanium alloys, Alpha 2 and Super Alpha 2, produced by Texas Instruments that retain their strength up to 1300°F and resist oxidation up to 1500°F.

The advantage that titanium alloys share over other alloys is that they have a natural layer of TiO2 over their entire surface. Other advantages of these alloys are that they have a lower density than superalloys, an ordered crystal structure, and a high specific creep strength. For these reasons titanium alloys were chosen as the structural material.

5.7. WEIGHT ANALYSIS

5.7.1. Introduction

Statistical weight analysis was performed on determining the Orbiter's dry weight (which also includes payload weight). This method involved comparative studies with the Boeing project and related hypersonic vehicle studies. The analysis also involved using experimentally derived weight estimation formulas from Nicolai that were to be pertinent to our Orbiter.

Our Orbiter, compared with that of Boeing's orbiter, was about 30 % less in volume and size. Also, the configurations between our Orbiter and Boeing's orbiter was similar. Both used a lifting-body geometry with two vertical stabilizers and the nose fuselage section was similar in shape and size. Given the similarities in design and mission, a statistical analysis was performed to see if a scaling system could be used to help in determining our Orbiter's weight.

The weight analysis also took into account whether or not there was enough volume for the various components, such as fuel, avionics, payload, cockpit, thermal system, propulsion, and structure. The main concern was the amount of volume that would be needed for fuel. This volume concern resulted from large amounts of hydrogen fuel that was needed for our orbiter. Therefore, an integral tank was used to minimize the volume.

Dry weight analysis was done for a full rocket system and for a scram/rocket system. The analysis showed that the rocket system used a lower dry weight due to its minimized flight time in the atmosphere. This is because the rocket system would have a much smaller thermal protection system, have a lighter propulsion system, and need less structural support since it would be in the atmosphere for a short time, about 1/2 the time for the scram/rocket system. The dry weight estimation between the scram/rocket and full rocket system was about 10,000 lbs. This was based upon the extensive analysis done on the scram/rocket system and then modifying this analysis for the full rocket system. Figure 5.7.1 shows the breakdown of various components for the scram/rocket system:

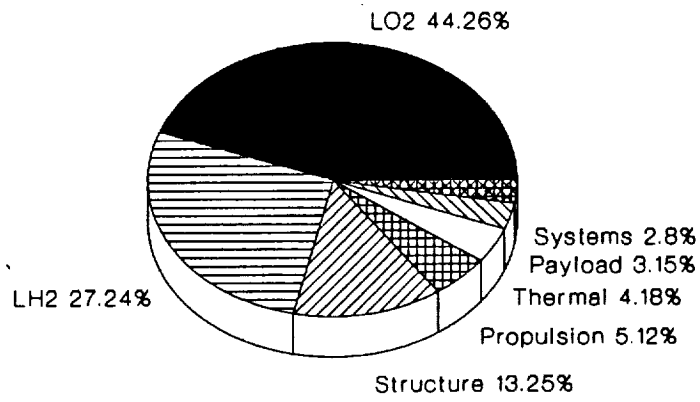

Figure 5.7.1. Orbiter Weight Statement.

The following is a weight breakdown for the scram/rocket system that was used for trajectory analysis:

System		Weight (lb)
Aerodynamic surfaces		4585.7
Fixed:	Wing	900.0
	Vertical Fins	2084.9
Movable:	Rudder	739.8
	Flaps	861.0
Body		36,570.4
Nose		1979.0
Front	LH2 Tank	13,283.0
	Mid LH2 Tank	5,069.9
	Aft LO2 Tank	4,905.9
Payload Bay		3664.1
Aft Body w/Thrust Structure		7668.5
Thermal System		11,191.8

Weight breakdown continued from above:

System	Weight (lb)
Landing Gears	2769.3
Manipulation of Payload	203.5
Propulsion System	16,240.7
Scramjets (8)	10,640.0
Inlets	2066.7
1/2 SSME	3534.0
RCS	1,555.0
Aero Controls	1,703.5
Guidance & Navigation	300.0
Instrumentation	300.0
Communication	220.0
Electrical System	2,650.7
Environmental Controls	399.1
Payload	10,000.0
Thrust Buildup/Pre-Ignition	500.0
Growth (2%)	1,800.0
Reserve fuel	2,000.0
Fuel	226,661.0
LH2	83,305.3
LO2	141,355.7
Dry Weight	90,339.0
Staging Weight	317,000.0

5.8. Ergonomics

The design of the cargo pod must allow for carry of ten crew members and various equipments. It must be able to support the life systems of the crew members and also take into account safety. The design of the foyer is for easy access and efficient use of space. The seats are designed for efficient use of space and give support to the crew members during acceleration. The cargo pod is able to be lifted out of the Orbiter's bay for ease of removal of large equipments.

Also, the hatches are designed, incorporating efficient use of available space. Life support systems are housed in the floor of the cargo pod and smaller equipments can be housed in the ceiling compartments, while larger equipments, such as satellites, engines, life support systems, etc...are stored in the rear half of the cargo pod. See Figure 5.8.1 and Figure 5.8.2, below.

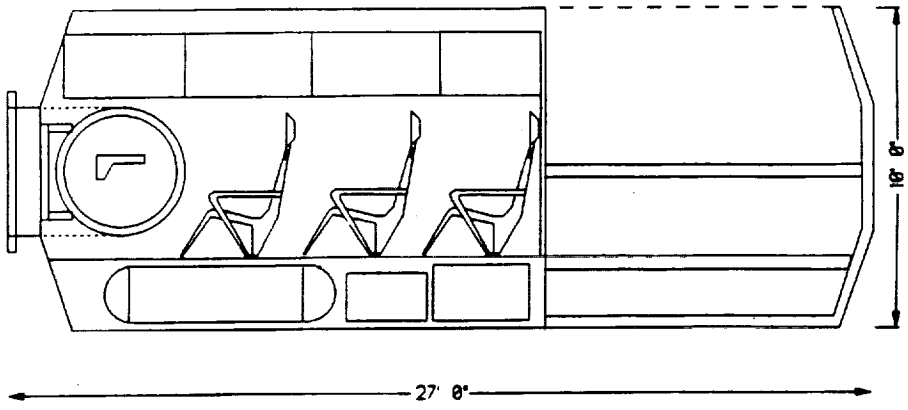

Figure 5.8.1. Preliminary Cargo Pod Design.

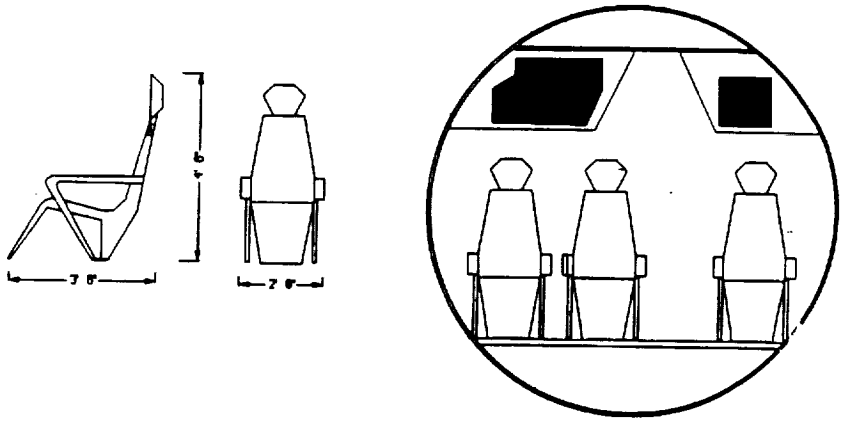

Figure 5.8.2. Preliminary Seat and Storage Arrangement.

Chapter 6 - Conclusions

Much work was completed in order to arrive at the two-stage to orbit configuration presented. It has undergone a number of changes since the beginning of the project, and a number of changes are still necessary.

Determining the initial staging Mach number was one of the most difficult parts of the project. Even at this point, the exact staging Mach number between Mach 6 and Mach 6.5 needs to be determined. In addition, the procedures at separation need to be planned and designed in more detail.

The trajectory analysis has come a long way since the beginning of the project. The current trajectory program is quite versatile, and can give accurate accelerations, velocities, and positions at any point in time if the propulsion and aerodynamic data is complete and accurate. The trajectory design can still be improved through further optimization.

The experiment-based aerodynamic data obtained for the carrier should be fairly accurate. More analysis and design needs to be completed in order to reduce the transonic drag, however, and more theoretical and experimental work with our configuration needs to be completed.

A fair amount of work went into deciding the fuel and engines to be used for our carrier. We are confident that liquid hydrogen fuel is the best for our design, and that tandem turbofan-ramjets are the best engine configuration. However, more work needs to be done on both the inlet and nozzle designs.

The weights and balances analysis indicates that the carrier needs to design more for trim conditions. The center of gravity and center of pressure need to be adjusted in order to allow the carrier to trim with less drag and less longitudinal stability. In addition, a complete stability and control analysis should be done for the carrier.

The orbiter's configuration employing airbreathers used less fuel than the full rocket configuration. The optimum staging velocity and altitude for minimum weight and the most simplicity for the system was a staging Mach number of 6 to 6.5 at an altitude of 90,000 ft.

Once it was decided that a scramjet/rocket system would be the propulsion unit for the Orbiter, thermal requirements dictated when the rockets should be turned on. We considered firing the rockets at Mach 15.5, thinking that the longer we used the scramjets the more fuel we could save. However, if the scramjets were employed too long, a heavier thermal protection system would be required, and a larger structural weight would be

incurred due to the large volume requirements of liquid hydrogen. This pushed the orbiter's dry weight above 100,000 lbs.

A Mach number of 12.3 seemed to be the optimum Mach number for firing the rockets. This gave us a smaller thermal protection system and a smaller volume of liquid hydrogen fuel, balancing the gains in weight from carrying more liquid oxygen. After doing statistical analysis with other similar orbiter models, we arrived at a dry weight of 90,339 lbs. This then gave us a staging weight of 317,000 lbs.

The integration of the scramjets into the fuselage was very important in our design. The scramjets were placed above the wings in order to allow them to be started before separating from the carrier. More work still needs to be completed on the scramjet integration.

The two stage to orbit concept seems to be a viable alternative to other systems currently under use and under study for the missions it is required to fulfill.

REFERENCES

1. Creel, Theodore R. Jr. and Jim A Penland. "Low-speed Aerodynamic Characteristics of a Hypersonic Research Airplane Concept Having a 70 Degree Swept Delta Wing." NASA TM X-71974, August, 1974.

2. Penland, Jim A., James B. Hallissy, and James L. Dillon. "Aerodynamic Characteristics of a hypersonic Research Airplane Concept Having a 70 Degree Swept Double-Delta Wing At Mach Numbers From 0.80 to 1.20, With Summary of Data From 0.20 to 6.0." NASA TP 1552, December, 1979.

3. Ellison, James C. "Investigation of the Aerodynamic Characteristics of a Hypersonic Transport Model at Mach Numbers to 6." NASA TN D-6191, April, 1971.

4. Clark, Louis E. and Christine B. Richie. "Aerodynamic Characteristics at Mach 6 of a Hypersonic Research Airplane Concept Having a 70 Degree Swept Delta Wing." NASA TM X 3475, May, 1977.

5. Truitt, Robert Wesley, Fundamentals of Aerodynamic Heating.

6. Hoff, Nicholas John, High Temperature Effects in Aircraft Structures.

7. Carroll-Porczynski, C. Z., Advanced Materials.

8. "Conceptual Design Aerodynamic Heating Analysis" (CDHEAT).

9. Anderson, John D., Introduction to Flight, McGraw-Hill, 1989.

10. Anderson, John D., Hypersonic and High Temperature Gas Dynamics, McGraw-Hill, 1989.

11. NASA TM X-3125, "Fail-Safe System for Actively Cooled Supersonic and Hypersonic Aircraft", 1975.

12. NASA TN D-2956, "Studies Relating to the Attainment of High Lift-Drag Ratios at Hypersonic Speeds", David E. Fetterman, Arthur Henderson Jr., Mitchel H. Bertram, and Patrick J. Johnson

13. John D. Anderson Jr., Modern Compressible Flow, McGraw-Hill, 1990

14. Hill, Philip G. and Carl R. Peterson, Mechanics and Thermodynamics of Propulsion, Addison-Wesley, 1965

15. Nicolai, Leland M., Fundamentals of Aircraft Design, Mets, Inc., San Jara, California, 1984.

16. Ellison, D.E., "USAF Stability and Control Handbook (DATCOM), "AF Flight Dynamics Lab., AFFDL/FDCC, Wright-Patterson AFB, Ohio, August 1968.

17. Bergmann, H. W. "Materials and Structural Concepts for New Space Transportation Systems." German Aerospace Research Establishment, 1989.

18. Sims, Hagel, and Stollof. Superalloys. Wiley Publishing, New York, 1989.

19. NASA - 1916. "Design Evaluation of Active Cooling..." Bell Aerospace Company.

20. 1990. Aviation Week and Space Technology, "Aerospace Materials." McGraw-Hill Pub., pg. 53-55.

Appendix A: Temperature Prediction Methodology

In order to determine the nose and leading edge surface temperatures during the carrier ascent to staging altitude and Mach number, a computer program was written to execute the following steps:

1. A data file was read which contained information concerning the carrier trajectory, namely the altitude and Mach number at 20 sec intervals during the flight.

2. Code utilizing the ARDC Standard Atmospheric Model was used to determine the temperature, pressure, and density from SL to 47km (154,000 ft) in 100m increments. These values are stored in memory for future use.

3. The heat transfer coefficient, h, was then determined for each time interval during the ascent. Thermodynamic properties were found at each point by taking the known altitude and linearly interpolating the ARDC data to find the temperature, pressure, and density at the desired altitude.

4. Once the values of h are calculated at each point along the trajectory, a Runge-Kutta routine is used to determine the surface temperatures of the leading edge and nose stagnation region at 20 sec intervals along the flight path.

The following equations were used in the computer code to determine the indicated variables:

For the ARDC Standard Atmospheric Model, for isothermal layers:

$$P/P1 = e^{-(g/RT)(h-h1)} = rho/rho1$$

for gradient regions:

$$P/P1=(T/T1)^{-g/Ar} \quad \text{where a=const}$$

$$rho/rho1=(T/T1)^{-((g/Ar)+1)} \quad \text{where a=const}$$

$$T=T1+a(h-h1) \quad \text{where h=altitude}$$

For the nose stagnation region, the heat transfer coefficient is given by:

$$h=f \cdot g \cdot Cp(\beta \cdot rho \cdot \mu).5$$
$$f=.763 \cdot Pr^{-.6}$$
$$g=32.2 \text{ ft/s}^2$$

Cp=specific heat of gas (.25 Btu/lb·°R)
β=3U/d where U=velocity
d=diameter of nose
rho=stagnation density at the nose
μ=viscosity at the stagnation temperature

When the freestream Mach number was supersonic, normal shock relations were employed to calculate the stagnation conditions and velocity behind the normal shock region in front of the nose.

For the leading edge, the heat transfer coefficient is given by:

$$h=hrt\cdot(3.18\cdot\cos 1.5Leff-1.55\cdot\cos 4Leff)\cdot Pf.8\cdot rle-.2f(Tw)$$

where:

$$hrt=.437\cdot(rho_\infty/rhoatm).78(V_\infty/104)1.54$$

$$Leff=\sin^{-1}(\sin L\cdot\cos\alpha)$$

L = sweep angle ($\approx 70°$)
α = angle of attack (assumed small)

$$Pf=\frac{1.33(M_\infty\cos Leff)^2+1}{(1.33\cdot M_\infty^2+2.5)(\cos^2 Leff+.00019)}$$

rle = leading edge radius

$$f(Tw)=1-.00013(Tw-1540)$$ Tw is in °F

The Runge-Kutta routine was set up as follows: for an equation of the form,

$$dy/dx=f(x,y)$$ b.c of (xo,yo)

$$yn+1=yn+1/6(k1+2(k2+k3)+k4)$$
$$k1=h\cdot f(xn,yn)$$
$$k2=h\cdot f(xn+\tfrac{1}{2}h,yn+\tfrac{1}{2}k1)$$
$$k3=h\cdot f(xn+\tfrac{1}{2}h,yn+\tfrac{1}{2}k2)$$
$$k4=h\cdot f(xn+h,yn+h)$$

where h is the interval between n values.